Article:
Yan, N, Colombera, L and Mountney, NP (2020) Three-dimensional forward stratigraphic modelling of the sedimentary architecture of meandering-river successions in evolving half-graben rift basins. Basin Research, 32 (1). pp. 68-90. ISSN: 0950-091X

https://doi.org/10.1111/bre.12367

THREE-DIMENSIONAL FORWARD STRATIGRAPHIC MODELLING OF THE SEDIMENTARY ARCHITECTURE OF MEANDERING-RIVER SUCCESSIONS IN EVOLVING HALF-GRABEN RIFT BASINS

Na Yan*[1], Luca Colombera[1], Nigel P. Mountney[1]

1 – Fluvial & Eolian Research Group, School of Earth and Environment, University of Leeds, Leeds, LS29JT, UK
* n.yan@leeds.ac.uk

ABSTRACT

The spatial organisation of meandering-river deposits varies greatly within the sedimentary fills of rift basins, depending on how differential rates of fault propagation and subsidence interplay with autogenic processes to drive changes in fluvial channel-belt position and rate of migration, avulsion frequency, and mechanisms of meander-bend cut off. This set of processes fundamentally influences stacking patterns of the accumulated successions. Quantitative predictions of the spatio-temporal evolution and internal architecture of meandering fluvial deposits in such tectonically active settings remain limited. A numerical forward stratigraphic model – the Point-Bar Sedimentary Architecture Numerical Deduction (*PB-SAND*) – is applied to examine relationships between differential rates of subsidence and resultant fluvial channel-belt migration, reach avulsion and channel-deposit stacking in active, fault-bounded half-grabens. The model is used to reconstruct and predict the complex morphodynamics of fluvial meanders, their generated channel belts, and the associated lithofacies distributions that accumulate as heterogeneous fluvial successions in rift settings, constrained by data from seismic images and outcrop successions. The 3D modelling outputs are used to explore sedimentary heterogeneity at various spatio-temporal scales. Results show how the connectivity of sand-prone geobodies can be quantified as a function of subsidence rate, which itself decreases both along and away from the basin-bounding fault. In particular, results highlight the spatial variability in the size and connectedness of sand-prone geobodies that is seen in directions perpendicular and parallel to the basin axis, and that arises as a function of the interaction between spatial and temporal variations in rates of accommodation generation and fault-influenced changes in river morphodynamics. The results have applied significance, for example to both hydrocarbon exploration and assessment of groundwater aquifers. The expected greatest connectivity of fluvial sandbody in a half-graben is primarily determined by the complex interplay between the frequency and rate of subsidence, the style of basin propagation, the rates of migration of channel belts, the frequency of avulsion, and the proportion and spatial distribution of variably sand-prone channel and bar deposits.

Keywords: Half-graben; meandering river; point bar; stacking pattern; sand connectivity; forward stratigraphic modelling.

INTRODUCTION

Rift basins developed in response to active extension commonly take the form of scoop-shaped depressions, bounded by normal faults that may penetrate as deep as to mid-crustal levels (Cowie *et al.*, 2000; Gawthorpe and Leeder, 2000; Moretti *et al.*, 2003; Ring *et al.*, 1992). The evolutionary history of such basins is recorded by the accumulated sedimentary lithofacies mosaics of the basin fill, which are influenced by depositional-system responses to tectonically induced tilting of the depositional surface and the generation of accommodation (Alexander and Leeder, 1987; Fraser *et al.*, 1997; Leeder and Gawthorpe, 1987). In rift zones, half-graben basins are characterised by a combination of footwall uplift and hangingwall subsidence, and usually comprise a narrow, steep footwall scarp slope along the fault zone and a gentler, broader hangingwall dip slope (Fig. 1) (Gawthorpe *et al.*, 1994; Gawthorpe and Leeder, 2000; Leeder, 2011; Leeder and Gawthorpe, 1987). Topographic tilting of the floor of such basins is associated with differential subsidence, whereby there typically exists a decrease of displacement both along the length of a basin-bounding fault from its centre to the fault tips, and also away from the fault to the basin margins. The displacement of a half-graben fault accumulates as the hangingwall pivots away from the footwall (Schlische, 1991). As a half graben develops, the pivot-like motion of the surface results from tilting by individual extensional episodes, which are associated with episodic seismic events (i.e. earthquakes) that generate accommodation. Ongoing sedimentation progressively fills this accommodation in the hangingwall of the basin (Bonini *et al.*, 2016; Gudmundsson *et al.*, 2013; Jackson, 1987; Marrett and Allmendinger, 1991). In sections aligned perpendicular to the trend of bounding faults, the fills of half-grabens commonly reveal thinning and onlap relationships against the hangingwall edge of the basin (Fig. 1), for example as seen on seismic reflection profiles like those from the Sevier Desert basin of Utah (McDonald, 1976) and the Fallon basin of Nevada (Anderson *et al.*, 1983). In continental half-grabens where fluvial systems occupy the basin floor, progressive tectonic tilting of the depositional surface acts to modify the existing floodplain topography of through-going river systems and superimposes a tectonic slope that strongly affects alluvial and fluvial processes within the developing basin (Gawthorpe and Leeder, 2000; Leeder and Alexander, 1987), thereby inducing lateral shift of the river in the direction of tilting.

Assessing and predicting lithological complexity in the fill of rift basins is important for two principal reasons: (i) it enables models to be developed whereby the sedimentary record can be used to reconstruct histories of basin evolution and to help assess the impacts of tectonic control on sedimentation; (ii) from an applied standpoint, the deposits of fluvial successions in rift basins form major oil and gas reservoirs (Corbett *et al.*, 2012; Hamdi *et al.*, 2014; Medici *et al.*, 2018b), serve as important groundwater aquifers (Lockwood, 2001; Medici *et al.*, 2016; Tellam and Barker, 2006), and act as potential sites for long-term carbon sequestration (Bachu, 2000) and for the underground storage of radioactive waste (Bath *et al.*, 2006; Medici *et al.*, 2018a). Point-bar deposits of meandering rivers are of particular importance in applied geology due to their economic potential as major hydrocarbon reservoirs (Jolley *et al.*, 2010; Larue and Hovadik, 2006).

In earlier attempts to investigate quantitatively the influence of tectonic controls on fluvial floodplain tilting and the associated architecture and channel-belt deposits of fluvial successions accumulated in half-grabens, a two-dimensional numerical model was used in

theoretical studies by Bridge and Leeder (1979), and further revised by Alexander and Leeder (1987). The model was later expanded to incorporate processes of river avulsion and lateral migration in three dimensions by Mackey and Bridge (1992, 1995). Modelling outputs associated with these studies show that the periodic tectonic subsidence causes axial river channels to reoccupy the position of the maximum subsidence to various degrees, which can then lead to a preferential stacking of alluvial sandbodies adjacent to the main fault zone.

However, these previous studies treated channel-belt deposits as homogeneous sandstones and disregarded the spatial heterogeneity of channel-belt deposits and associated variability in stratal geometries and sedimentary architectures. These factors may potentially play an important role in influencing the connectivity, i.e., the property of being connected, of relatively more porous and permeable deposits in half-graben basins.

This study utilises the basin-fill modelling capabilities of a three-dimensional forward stratigraphic model, the Point-Bar Sedimentary Architecture Numerical Deduction (*PB-SAND*). The aim of this study is to document the effect of repeated fault-slip events associated with development of a half-graben on the three-dimensional distribution and stacking patterns of fluvial meandering channel belts and their deposits at different spatial and temporal scales. Detailed research objectives are as follows: (i) to examine how the magnitude of fault-controlled subsidence and associated frequency of periodic fault slip control stratal geometries and facies stacking patterns of axial fluvial channel-belts in a half-graben basin; (ii) to quantify how sandbody connectivity changes along and away from the basin-bounding fault; and (iii) to demonstrate how forward stratigraphic modelling outcomes can assist predictions of the three-dimensional distribution of fluvial deposits and aid in reconstructing scenarios of basin evolution.

BACKGROUND

The frequency and magnitude of fault slip strongly controls the spatial distribution of lithofacies and architectural elements (and thereby lithological heterogeneity) within a rift basin, and stratigraphic variations in the stacking patterns of sedimentary bodies (Einsele, 2013; Withjack *et al.*, 2002). Processes of lateral channel migration and avulsion can have a significant impact on the distribution and relative proportion of lithofacies, and geometry, stacking patterns, and connectivity of channel deposits.

Differential subsidence caused by tectonic tilting in an extensional half-graben creates a surface topographic gradient and exerts impact on the behaviour of active fluvial systems within the basin, and thereby influences the mechanism of accumulation and three-dimensional architecture of sedimentary elements that comprise such fluvial systems (e.g. channels, bars, splays). Such controls on fluvial systems are recorded in the stratal geometry of the basin fill as complex distributions of lithofacies and architectural elements (Biswas, 2003; Mack and Leeder, 1999; Peakall, 1998). The evolution of fluvial meandering rivers and the distribution of channel-belt deposits, in particular, are controlled by spatial and temporal variations of accommodation generation and basin physiography, arising from differences in fault slip rates and local subsidence, and influencing local river-channel gradient. The importance of tectonic tilting on the behaviour of axial rivers has been well documented (Coleman, 1969; Fisk, 1944; Leeder and Alexander, 1987; Peakall, 1998; Peakall *et al.*, 2000). The development of topographic gradient that is normal to the strike of basin-bounding faults influences the local

direction of flow and rates of lateral migration of axial rivers, and encourages channel belts to shift towards the position of topographic minimum, i.e., the site of maximum subsidence adjacent to the main fault (Alexander and Leeder, 1987; Leeder and Alexander, 1987). Rivers shift position through lateral channel migration that proceeds through multiple episodes of meander migration and cut-off, or by channel avulsions (Fig. 1). The progressive migration of channels can result in the development of a broad channel belt in which remnant abandoned channel and point-bar elements record a progressive shift in the position of the belt towards the locus of subsidence (i.e. towards the basin-bounding fault). Within such belts, older meander loops are preferentially abandoned on the side of the belt farther from the faulted basin margin. This process, known as 'lateral channel combing', is seen in modern rivers flowing through extensional basins, such as the South Fork Madison River of Montana (Alexander *et al.*, 1994; Leeder and Alexander, 1987), the Mississippi River in the New Madrid area (Alexander and Leeder, 1987; Russ, 1982), and the Owens River of California (Reid and John, 1992). Meanwhile, active river reaches are prone to nodal avulsions (Alexander and Leeder, 1987; Armstrong *et al.*, 2014; Dixon *et al.*, 2018) that result in episodic shifts of entire sections of channel-belt towards the main basin-bounding fault. The incidence of down-tilt avulsion episodes is known to increase in frequency in response to fault movement, as in the Carson and Walker River in Nevada (Peakall, 1998; Peakall *et al.*, 2000).

Tectonic tilting and the associated patterns of subsidence and uplift in a half-graben system exert a profound control on the sediment-transport pathways, distribution of lithofacies, stratal geometry, and facies stacking pattern. The influence of tectonic tilting is further complicated by the history of the fault itself: processes of fault propagation, growth, linkage, and death (Dawers and Anders, 1995; Gawthorpe and Leeder, 2000; Kim and Sanderson, 2005). The boundaries of fault segments are delineated by local highs and lows in hangingwall and footwall elevations, respectively (Fig. 1). The growth and development of a fault leads to spatial variations in subsidence and accommodation development. To better understand how fault geometric parameters tend to co-vary, and how they evolve over time, many studies have examined relationships between the maximum displacement and length of faults, mostly through combination of different field and reflection-seismic datasets. A general consensus is

Fig. 1. Schematic diagram of an evolving half-graben basin in a fluvial-dominated continental setting. (A) Section through part of a half-graben basin. The rate of subsidence is at a maximum at a position adjacent to the fault in the centre of the basin; subsidence decreases to zero at the basin edges. An axial river runs through the basin close to the line of the fault. *L* is the length of the fault. *D* is the accumulative displacement. (B) Stacking of channel-belt deposits that are controlled by the generation of accommodation and the presence of a surface gradient induced by tectonic tilting. The location of channel belts developed following avulsion events is determined by the location of available accommodation, which itself is a function of tectonically induced subsidence and the distance from previously deposited channel-belt accumulations. Meanwhile, the minimal distance that channel belts can encroach towards the fault is restricted by the toes of alluvial fans that form a bajada along the line of strike of the fault. (C) Architecture of channel-belt deposits. Controlled by tectonic tilting, axial rivers tend to migrate toward the fault zone within an evolving rift basin, resulting in preferential preservation of older abandoned channel-fill elements in an up-tilt direction. This pattern of preservation is a common feature of preferentially directed channel combing. Note the pattern of stacking and aggradation of older channel-belt deposits. (D) A representative cross section in the transverse direction of a channel-belt accumulation. (E) A representative cross section in a direction parallel to the trend of the channel-belt. Typical fining-upward lithofacies successions are shown in the cross sections. (F) Typical grain-size profile of a vertical cross section of a point-bar deposit. Note vertical scales are highly exaggerated. D-F modified in part from Ghazi and Mountney (2009). See text for further explanation.

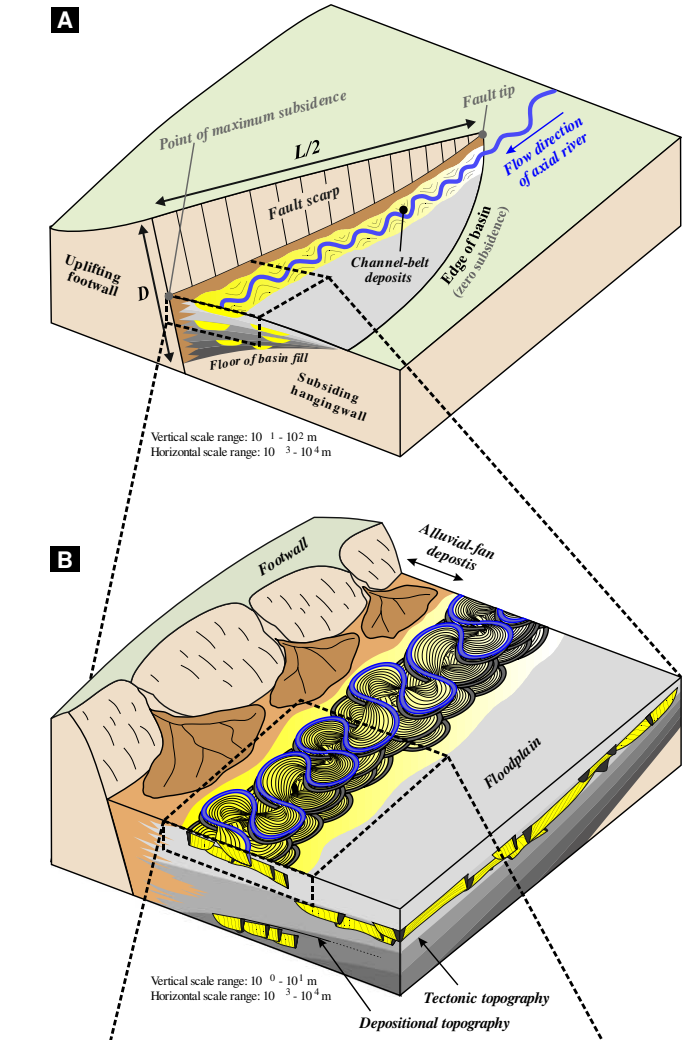

Simulation of basin evolution and accommodation generation

HALF-GRABEN DEVELOPMENT

- parabolic plan-view shape
- periodic fault slip, with Weibull distribution of slip period
- linear decrease in fault displacement both along and perpendicular to boundary fault
- scaling between fault displacement and length

Simulation of controls on channel-belt stacking

CONTROLS ON CHANNEL-BELT LOCATION

- avulsion controlled by tectonic tilt
- channel-belt compensational stacking
- repulsion by footwall-hosted alluvial fans

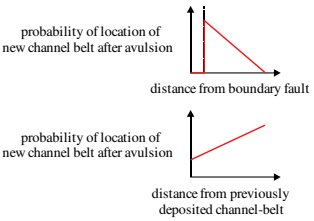

Simulation of channel-belt facies architecture

INTERNAL ARCHITECTURE

- tilt-induced channel combing
- channel-belt aggradation, proportional to accommodation
- amalgamation resulting from channel cutoffs
- stratal geometries resulting from styles of meander transformation and channel planforms

FACIES DISTRIBUTIONS

- point-bar and channel-fill lithologies
- vertical trends in point-bar lithofacies
- horizontal trends in point-bar lithofacies, reflecting spatial variations (around meander bend) and temporal variations (as meander bend evolves)

that there is a scaling relationship between the total cumulative displacement (D_{max}) and the maximum trace length (L) of a fault, through a relationship of the type:

$$D_{max} = C\,L^{n}$$

where C is a constant related to rock properties and tectonic environment, and n is an exponent ranging between 1 and 2 (Cowie and Scholz, 1992; Dawers and Anders, 1995; Dawers *et al.*, 1993; Gillespie *et al.*, 1992; Kim and Sanderson, 2005; Marrett and Allmendinger, 1991; Nicol *et al.*, 1996; Pickering *et al.*, 1995; Schlische *et al.*, 1996; Scholz and Cowie, 1990; Walsh and Watterson, 1988; Watterson, 1986). Many researchers argue that faults are scale-invariant and the maximum displacement increases linearly with the fault length, i.e., $n \cong 1$ (Bonini *et al.*, 2016; Carter and Winter, 1995; Clark and Cox, 1996; Cowie and Scholz, 1992; Dawers and Anders, 1995; Dawers *et al.*, 1993; Schlische *et al.*, 1996; Scholz *et al.*, 1993; Villemin *et al.*, 1995). Some studies, on the contrary, argue that the styles of fault growth essentially indicate the maturity of a fault (Walsh *et al.*, 2002). Although active faults may propagate along their entire perimeter and grow in strike length rapidly during the early stages of fault growth (Filbrandt *et al.*, 1994), large faults tend to be confined laterally and the fault length remains almost constant as displacement accumulates (Gross *et al.*, 1997; Walsh *et al.*, 2002), for example as seen in many large Holocene normal faults in Iceland (Gudmundsson, 2005; Gudmundsson *et al.*, 2013). Furthermore, the linkage of adjacent smaller faults into a larger fault is another important mechanism by which a fault grows (Cartwright *et al.*, 1995; Gawthorpe and Leeder, 2000; Peacock, 2002; Peacock and Sanderson, 1996; Segall and Pollard, 1980). The progressive growth of an isolated half-graben is the focus of this study, and fault growth by lateral linkage is therefore not considered further here.

METHODOLOGY

Approach to modelling half-graben basin evolution

As a fault evolves with or without lateral growth, the total displacement of the fault accumulates by episodic slip events that are often associated with seismic activity (Bürgmann *et al.*, 1994; Cowie and Scholz, 1992; Walsh and Watterson, 1987). Based on observations that the likelihood of an earthquake increases progressively with time as crustal strain accumulates since the release of strain by the previous earthquake (Bridge and Leeder, 1979; Hagiwara, 1974), the period of seismic events is modelled using a two-parameter Weibull probability density function, which takes the form:

$$f(t) = \frac{c}{\eta}\left(\frac{t}{\eta}\right)^{c-1} e^{-(t/\eta)^{c}}$$

and

$$\overline{T} = \eta\,\Gamma\left(\frac{1}{c} + 1\right)$$

where c is the shape parameter, equal to 2 by default, in line with Bridge and Leeder (1979), η is the scale parameter, $\overline{T}$ is the mean of the distribution, and Γ is the gamma function. A histogram of slip periods with a Weibull distribution fit is shown in Fig. 2A. The maximum displacement at each slip (d_{max}) event is determined by:

$$d_{max} = v\,t$$

where v is the average slip rate, sampled using the Monte Carlo method from a predefined probability distribution (e.g., Normal distribution), and t is the time period between two successive tilting events that is sampled from a predefined Weibull probability density function. All samples from predefined probability distributions are independent with each other. A modelling example of basin growth induced by episodic slip events is shown in Fig. 2B, in which fault slip is assumed to be periodic, and a mean slip period of 800 years is used with a range of 100 - 2000 years, which is consistent with the mean recurrence period of 10^1 - 10^3 years for earthquakes larger than a magnitude of 6 in tectonically active areas (Bridge and Leeder, 1979).

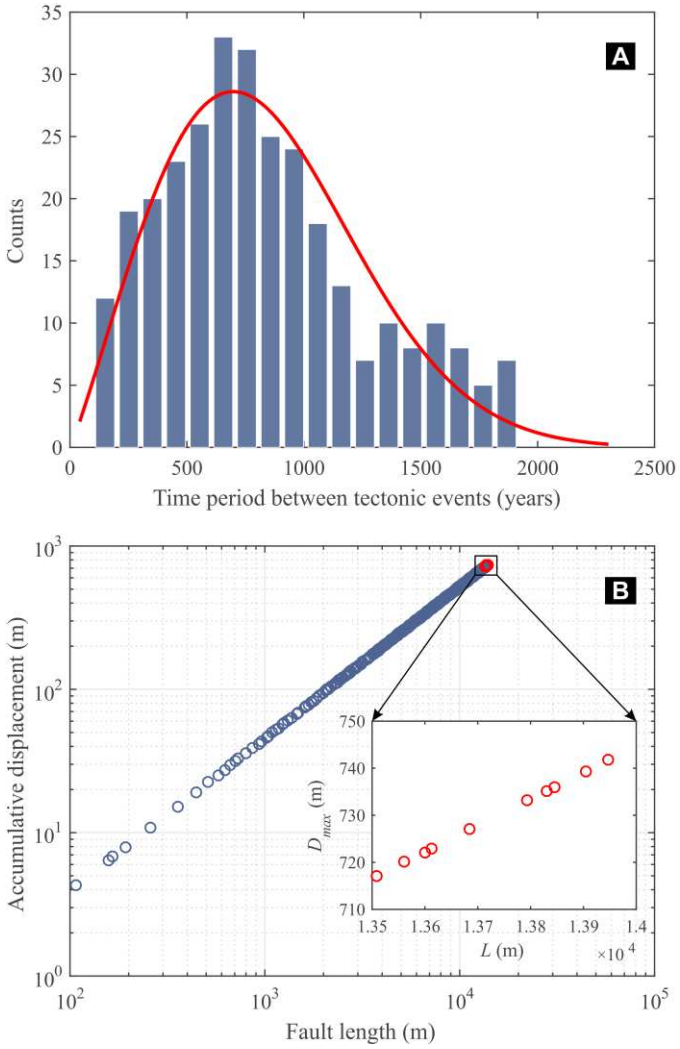

Fig. 2. (A) Histogram example of the period of tectonic events, with a fitted Weibull distribution. Three hundred samples are randomly selected from a Weibull distribution of c = 2 and $\overline{T}$ = 800 yrs. with minimum and maximum cut-offs of 100 years and 2000 years, respectively. (B) A modelling example generated to show the growth of an isolated basin, using the relationship between fault length and accumulative displacement found in Schlische *et al.* (1996). The v is sampled from a normal distribution with a mean of 0.003 m yr^{-1} and 3σ of ±0.002 m yr^{-1}, within the range of rates reported from normal faults in the continental settings (Gawthorpe *et al.*, 1994, Machette *et al.*, 1991). Red circles and the inserted graph denote the ten most recent slip events.

The plan-view geometry of a half-graben basin is modelled using a parabola with the vertex at the point where the hinge of the hangingwall rollover is farthest from the fault (Fig. 1A). Meanwhile, the displacement along the fault is also modelled using a parabola with the vertex at the fault centre where the maximum displacement occurs. The displacement perpendicular to the fault decreases linearly away from the fault to the basin edge (i.e. the position of zero subsidence). The combination of displacement change along the strike of the fault (i.e. parallel

to the trend of the fault) with the linear decrease of displacement perpendicular to and away from the fault generates the scoop-shaped basin geometry typical of half-grabens. The lateral propagation and growth of a fault can be modelled and constrained based on the relationship between the total accumulated displacement and strike length discussed previously. The point of maximum displacement is kept fixed; the associated hinge point of the hangingwall rollover may, however, migrate away from the fault as the fault grows by radial extension (Kim and Sanderson, 2005). Modelled examples of faults developed through four different propagation mechanisms are shown in Fig. 3. The growth style of a single isolated fault depicted in the upper two panels in Fig.3 is akin to that of mature faults described by Walsh *et al.* (2002), whereby the length of the fault remains constant as displacement accumulates, and whilst the hinge of the hangingwall rollover is fixed (the left panel) or migrates (the right panel). In contrast, the growth style of the faults depicted in the bottom right panel resembles active faults at their relatively early stage of development with basin boundaries propagating along their entire perimeter (Filbrandt *et al.*, 1994). The bottom left panel depicts the case of a fault that grows in length while the width of the basin remains constant. In reality, a fault is likely to experience multiple stages of development, with alternation of the different growth styles represented in Fig. 3. In the results presented subsequently, the style of basin growth represented in the bottom rigth panel is modelled, whereby the fault propagates laterally with a gradual growth in length, and the hinge of the half-graben rollover moves away from the fault; this dynamic results in onlapping stratal terminations against the hangingwall, as commonly recognized in reflection-seismic datasets (e.g., Schlische and Anders, 1996; Schlische and Olsen, 1990; Withjack *et al.*, 2002).

The modelled basin is ~12 km long and ~7 km wide, growing along its entire perimeter by radial extension of the basin edges (Filbrandt *et al.*, 1994); the chosen size is comparable with that of typical half-grabens, which commonly range from 12 to 50 km in length and from 5 to 20 km in width (Gawthorpe *et al.*, 1994; Leeder *et al.*, 1996). The half-graben is modelled as growing episodically over time, triggered by multiple slip events. Ten increments of basin infill are modelled to reveal the expected fluvial sedimentary architecture arising as part of a rift-basin fill. Each of the 10 increments represents a stratigraphic interval developed in response to one slip event on the basin-bounding fault. The cumulative displacement and the length of the modelled fault induced by the ten episodic slip events are presented in Fig. 2B (see red circles in the insert panel).

Fig. 3. Different evolution styles of individual fault-bounded half-graben basins, from PB-SAND modelling examples. The development of individual faults is induced by episodic slip events. The ten most recent stratigraphic intervals representing the accommodation generated by tectonic events are shown in 3D and frame diagrams. The slip period associated with tectonic events is modelled using a Weibull distribution. Cross sections *A-A'* and *B-B'* in each of four cases show subsidence change along the fault zone and transverse section perpendicular to the fault, respectively. The graded colour denotes fault boundaries by each slip event; black and blue axes denote the direction of *x*- and *y*-axes, respectively. As subsidence increases, a basin changes in shape depending on whether the fault extends laterally and whether the hinge point of the hangingwall rollover migrates away from the fault. Four end member basin evolution types are depicted: constant fault length and fixed hinge point (top left); constant fault length and migrating hinge point (top right); growing fault length and fixed hinge point (bottom left); growing fault length and migrating hinge point (bottom right). It is this latter case that is employed in the modelling used for this study. The vertical axes (elevation) are highly exaggerated. No specific scale implied for these conceptual models. See text for further explanation.

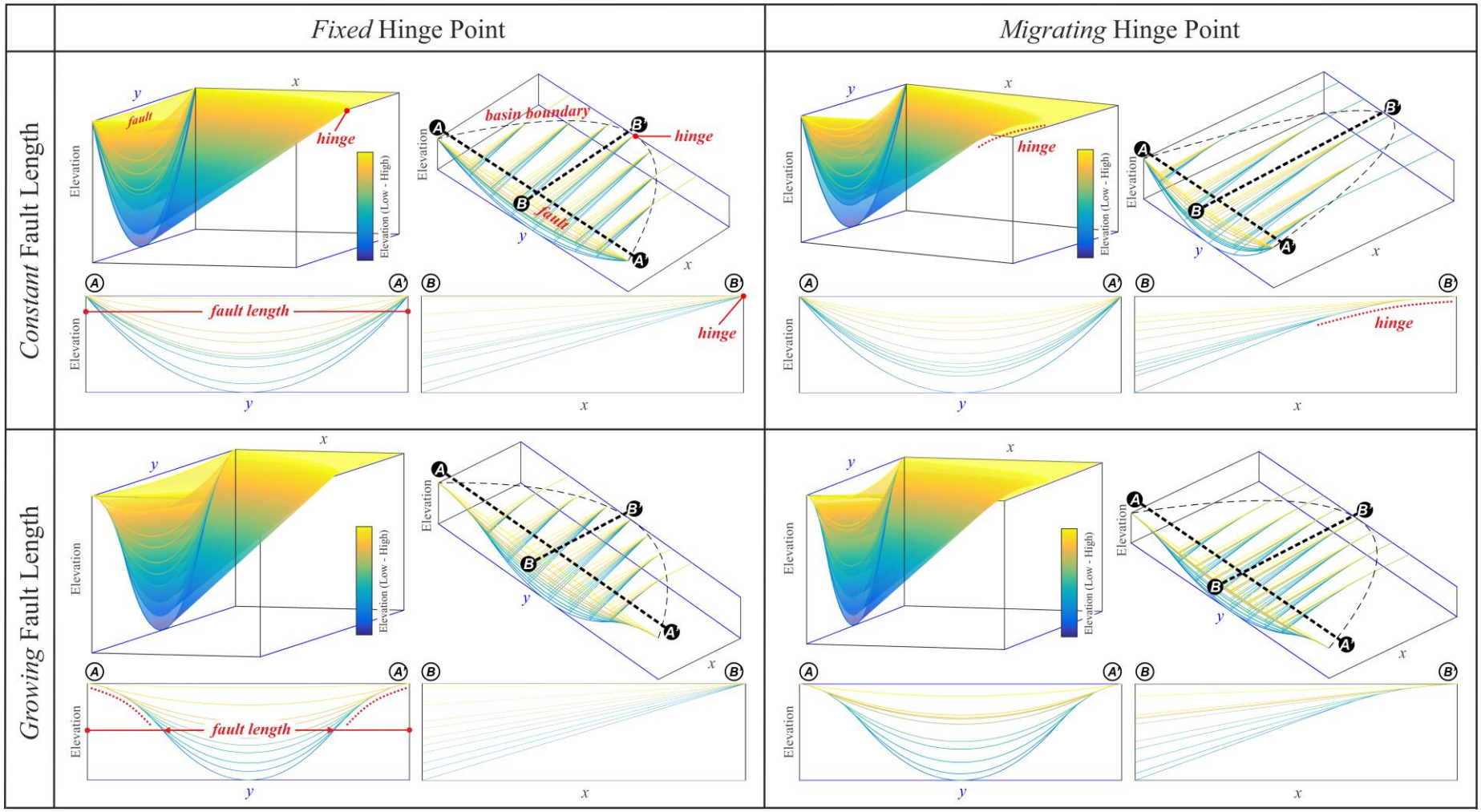
Fixed Hinge Point
Migrating Hinge Point
Constant Fault Length
Growing Fault Length
fault
hinge
basin boundary
fault length
Elevation
Elevation (Low - High)
x
y
A
A'
B
B'

Approach to modelling fluvial-system evolution within a half-graben basin

Three aspects of fluvial sedimentary architecture in an evolving half graben are considered in detail in the model: (i) the plan-form morphology of an active river with multiple meander bends that themselves evolve through varying transformation styles; (ii) the different patterns of channel-belt deposits that arise from the repeated shifting of river channels through lateral migration, cut-off and avulsion; (iii) stacking patterns of elements and facies that arise in response to rates of accommodation generation that vary both temporally and spatially in an evolving half graben.

The plan-view morphology of a single fluvial channel representing a river flowing axially through a half-graben basin is generated by selecting a combination of idealised and/or real-world examples of channel trajectories associated with three consecutive meander bends, each stored in a library of mutually compatible planforms. Modelled examples of single channel belts comprising point bars and channels with different planform morphologies are shown in Figure 4. Facies distributions and sedimentary architectures of point-bar deposits are closely related to the growth histories and transformation styles of point-bar development (Ghinassi *et al.*, 2014). A more detailed explanation of the algorithms of the *PB-SAND* model can be found in Yan *et al.* (2017). *PB-SAND* is a geometric 3D forward stratigraphic model that is vector based.

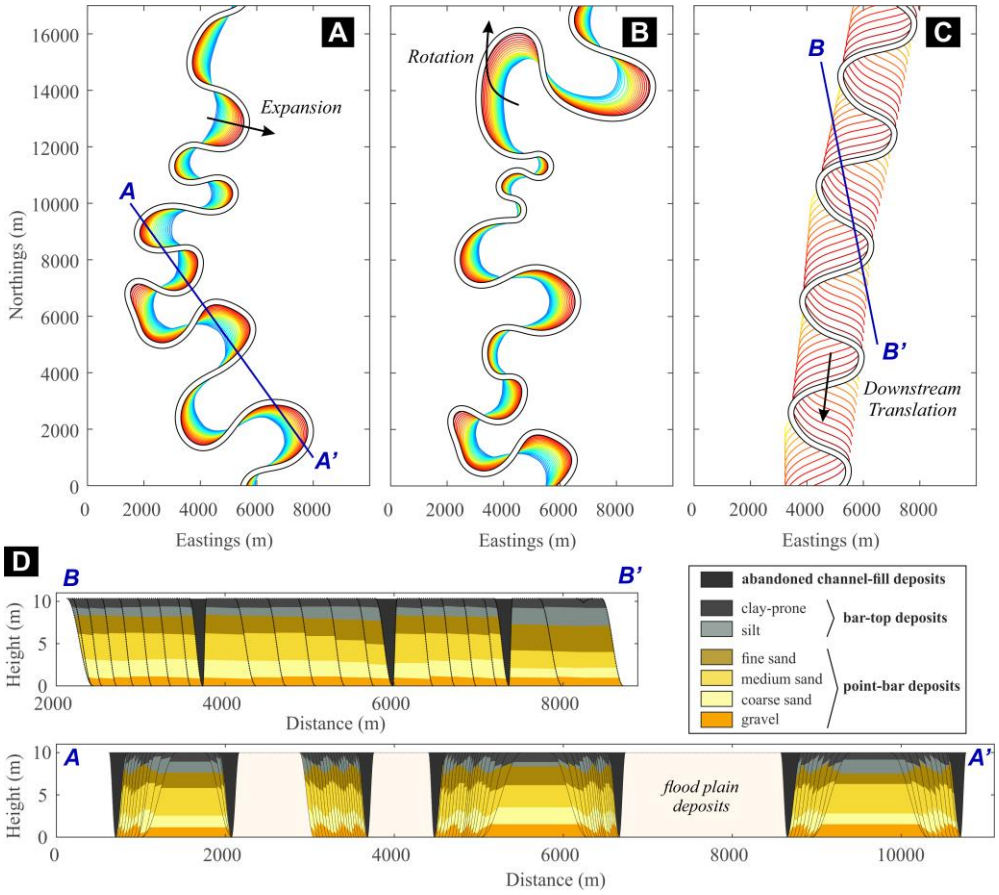

Fig. 4. Modelling examples of meandering rivers. The algorithm can simulate point-bar elements with different transformation styles (e.g., expansion, rotation, and downstream translation), sinuosity, geometry, and vertical and horizontal facies trends. A particular river reach can be modelled by combining multiple meander bends in sequence, and can be constrained on planform observations from modern rivers, reflection seismic images, or rock outcrops. Examples of cross sections are also presented.

The planform fluvial morphologies and architectures generated by the model can be constrained with seismic and outcrop-analogue data. The model allows generation of sedimentary architectures resulting from different styles of meander transformations, while simultaneously maintaining small-scale facies characteristics of intra-bar deposits (Colombera *et al.*, 2018; Yan *et al.*, 2019). In this study, to minimise the number of variables used in the model, a simple planform pattern that incorporates typical expansional and rotational point-bar elements (see details in Yan *et al.*, 2019) is used as a template for generating channel reaches. We chose the simple shape of a "classic" expansional and slightly rotational point bars since such bar types are representative of many meandering rivers generally. The choice to model this shape of point bar was deliberate to minimize the number of parameters that can vary in the model. This has allowed us to focus specifically on an analysis of larger-scale stacking patterns of channel belts in a half-graben setting, rather than having to explain the many parameters that can be used in PB-SAND to model smaller-scale point-bar morphologies and evolutionary trajectories, the effects of which on resultant sedimentary architecture are minimal at the channel-belt scale. For similar reasons, we also chose not to model the effects of meander loop cut-offs; although the PB-SAND model is capable of modelling such behaviour, its inclusion adds considerably to run times yet results in channel-belts sedimentary architectures that are similar to those that do not include loop cut-offs.

The width of a channel belt, including active and abandoned channel fills and bars, is modelled by *PB-SAND* and is dependent on (i) the size of a river, (ii) the length of time over which the river migrates, which itself is controlled by avulsion induced by episodic tectonic events, i.e. time period (t) between two successive slips, and (iii) the river migration rate, which is related to the gradient created by topographic tilting, and which drives preferential channel migration towards the fault zone, thereby increasing the channel-belt width and the abandonment of meander-loops up-tilt via cut-offs or avulsions. Furthermore, a slope threshold of 0.015° (i.e. the slope of central cross section at the maximum subsidence) is defined below which a channel migrates or avulses randomly (either towards or away from the fault zone) and no preferable migration occurs. In vertical section, the thickness of channel belts and aggradation are controlled by the accommodation generation rate (Fig. 1C). The modelling approach used here is set such that the rate of river aggradation keeps up with the rate of subsidence (i.e. the accommodation generated by a fault-slip event is fully consumed by sedimentation before the following slip event takes place). Thus, the evolving basin is in a 'filled' state whereby no available accommodation remains and the surface of the basin has now tectonically induced gradient (*cf.* Banham and Mountney, 2013). The hydraulic geometry of channels remains the same at the modelled temporal scales (a slip period of tens to thousands of years) (Bridge and Leeder, 1979; Stouthamer and Berendsen, 2001). In PB-SAND, it is possible to model continuous basin aggradation simultaneously to river migration (Fig. 5); however, a more computationally efficient solution is used in the results presented next, consisting of the step-wise vertical shift of the point bars that compose the amalgamated channel belts; the choice of this solution does not affect the overall large-scale stacking patterns of channel-belt deposits in the basin. Examples of channel belts developed through random vs. preferable (i.e. tilt-induced) migrations are demonstrated in Fig. 6. As the gradient in the left part of the image in Fig 6A is larger than the threshold of preferable migration, the channel belt shows a gradual migration to the left and combing geometries of abandoned channel elements are preferentially

accumulated on the upslope. By contrast abandoned channels are located on both sides of the channel belt in Fig 6B due to the absence of a transverse gradient.

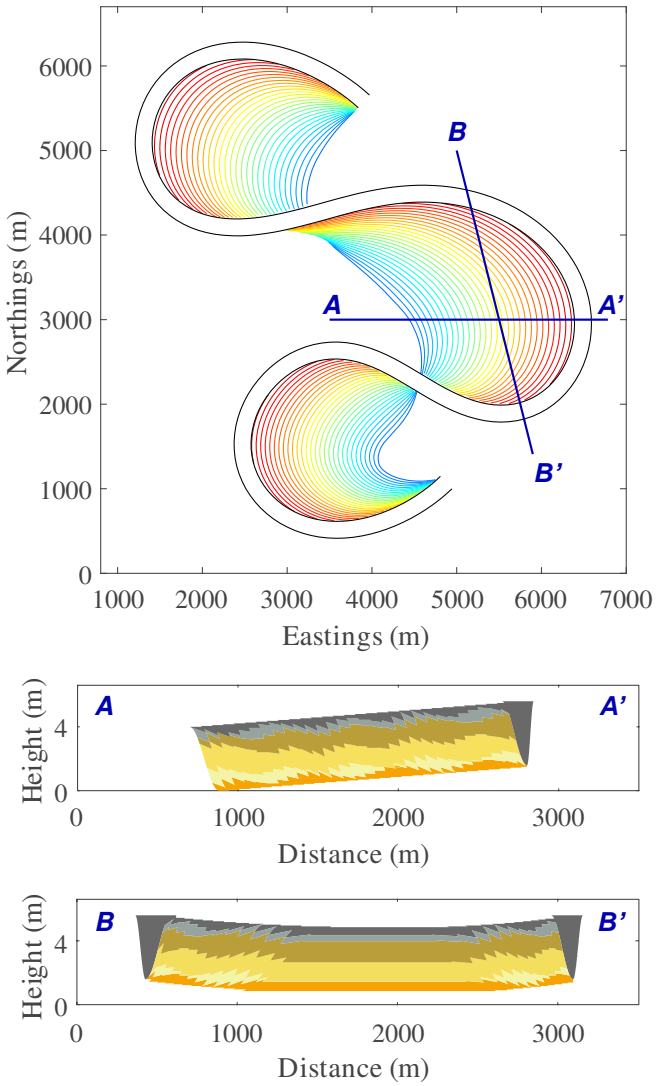

Fig. 5. An example of modelled point bars showing gradual aggradation over time. The two cross sections *A-A'* and *B-B'* show linear aggradation, i.e., a constant relationship between basin aggradation rate and river migration rate, but temporal variations in aggradation rate can also be modelled by PB-SAND.

Avulsion is modelled as occurring episodically following each slip event and in a way that allows for the channel to shift to any favourable position on the floodplain surface (Fig. 7). Avulsion-driven jumps in channel position are obtained by Monte Carlo sampling from a probability distribution. The location of the newly developed channel belt after an avulsion event triggered by seismic activity is determined by (i) the tectonic gradient caused by hangingwall tilting, which by default is a linear increase in probability towards the fault zone so as to model channels that preferentially migrate towards the locus of subsidence, and (ii) the relative distance from the location of the previous channel belt that was generated immediately before the avulsion event occurred, which by default is a linear increase in probability away from the channel belt to mimic the influence of elevated channel ridges on avulsion position (Fig. 1B). This latter condition enables the model to mimic post-avulsion channel-belt locations that account for compensational stacking of channel-belt deposits (Hajek *et al.*, 2010). Furthermore, fans that are sourced in the footwall typically push the axial-river path away from the fault-bounded basin margin (Alexander and Leeder, 1987). The

influence of footwall-sourced fans is accounted for in the model by specifying a buffer zone within which channel belts do not develop, so as to mimic the effects of fan toes. In the simulations described below, the buffer zone is kept constant along the fault, with a width of 200 m.

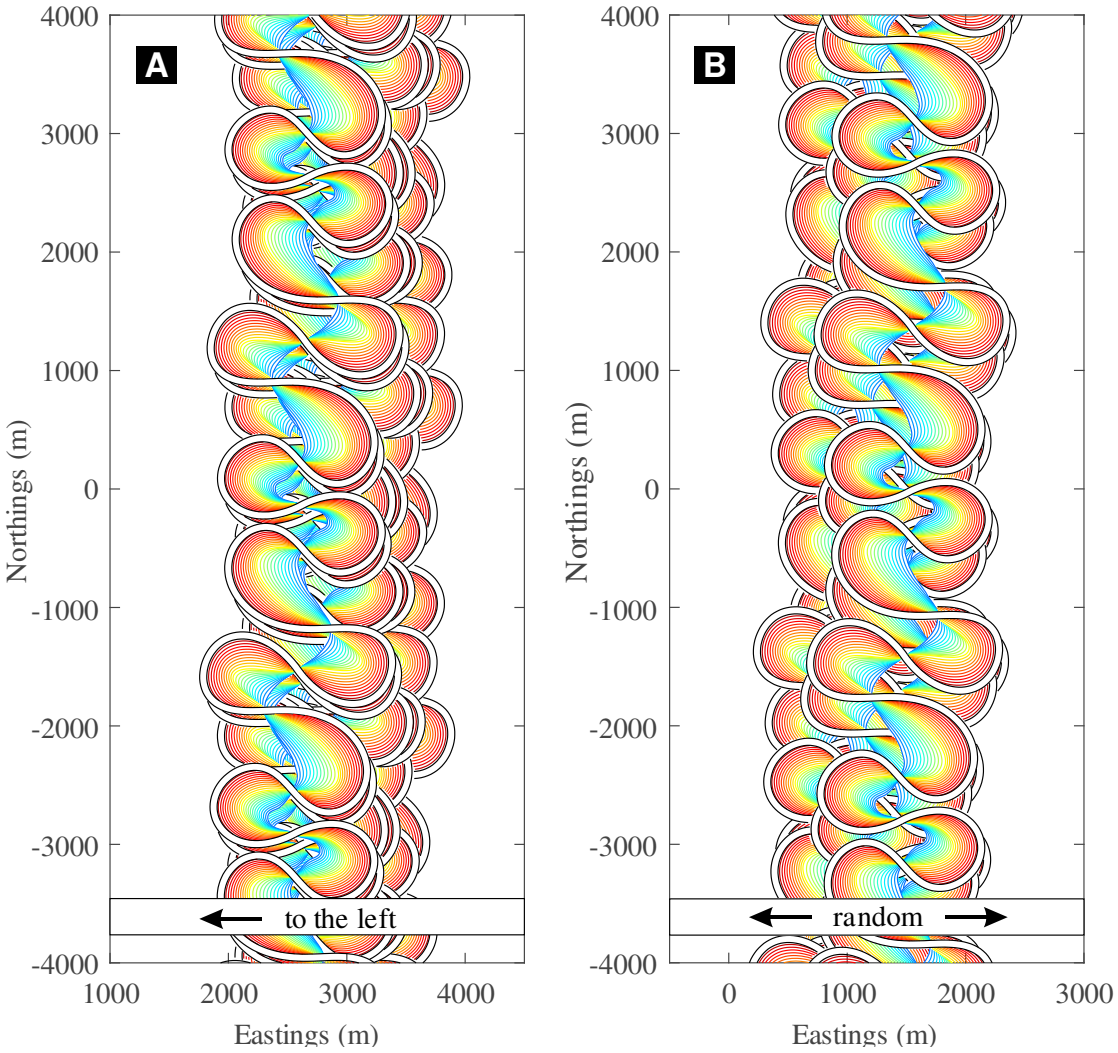

Fig. 6. Modelling examples of meander belts caused by different styles and rates of channel migration associated with different degrees of displacement by tectonic activity. Channel migrates preferably towards the depocentre (A) or randomly (B). The lateral migration rate is controlled by local gradients induced by tectonic tilting.

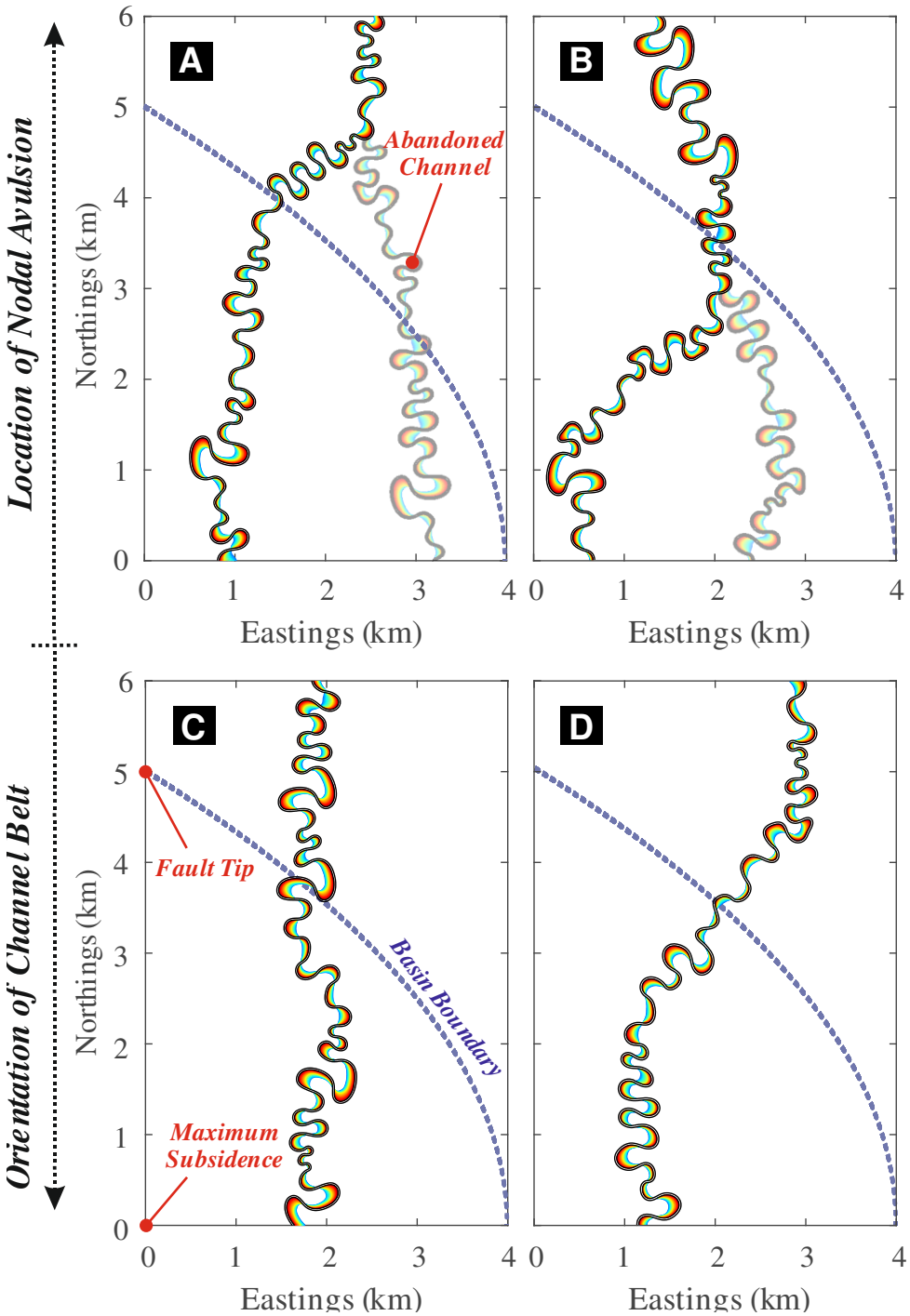

Fig. 7. Modelling examples that illustrate how model set ups can vary with respect to (i) position of the location of an avulsion node (A, B) and (ii) a fixed or changing orientation of the channel belt (C, D). The river planform geometries are modelled by randomly selecting and arranging point bars from ten real-world case examples in a library. Nodal avulsions can be modelled to either occur outside of the basin (A), or within the basin (B). The model can also be run in such way that the orientation of channel-belt axes is constant and parallel to the basin-bounding fault (C) or is influenced by tilt-induced gradients (D). In this work, outputs are shown for model runs corresponding to scenarios represented in A and C, for computational efficiency, although scenarios B and D might also be common in nature. Cases A and C are common in rift basins where the rate of infilling of accommodation generated by fault-induced subsidence is near instantaneous. In such circumstances, the basin is effectively filled and the gradient across the basin floor is not significantly affected by the locus of maximum subsidence at the basin centre.

MODELLING RESULTS

The facies stacking patterns of channel belts developed in an evolving half-graben are examined in this section. An example of the resulting stratigraphic intervals accommodated by the ten slip events are shown in Fig. 8A, which depicts selected 2D cross sections from the overall 3D model output. Representative cross sections perpendicular to the fault and their associated basin edges are also outlined in the frame diagram with different colours in Fig. 8B.

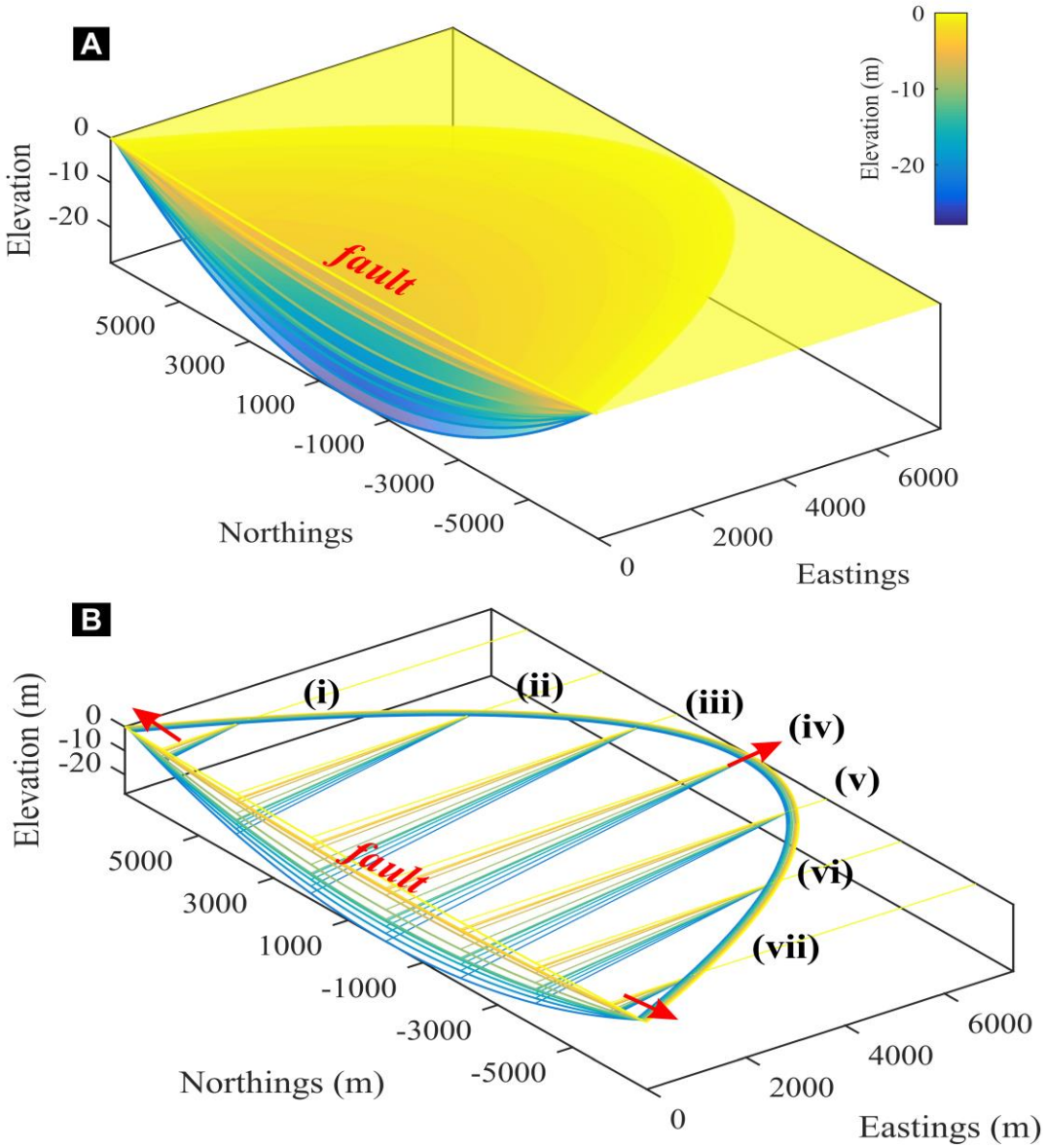

Fig. 8. (A) An example of ten stratigraphic intervals representing increments of accommodation generation and basin fill, modelled in an evolving half graben shown in 3D view. (B) Frame diagram showing sedimentary units employed by ten episodic seismic events (denoted by different colours). Red arrows show the growth direction of the evolving basin.

The accumulated fluvial point-bar elements that comprise the deposits of the channel belts have been modelled as having simple forms developed through expansional and rotational meander transformations (Fustic *et al.*, 2012; Ghinassi and Ielpi, 2015; Ielpi and Ghinassi,

2014; Russell *et al.*, 2019). The model, however, is capable of modelling point-bar elements developed through more complicated meander-bend transformation behaviour (Fig. 4). The primary parameter settings are summarised in Table 1. Figure 9A shows the width of channel belts and their location relative to the fault and basin edges; the channel belts are numbered 1 to 10 in chronological order. Red arrows denote the direction in which the rift basin is growing at the modelled temporal scale of ~10^4 years (ten slip events). Figure 9B shows examples of three of the resultant modelled channel belts in plan-view. Although the channel belt 3 (*CB_3*) and 8 (*CB_8*) are similar in development time (~800 yrs.), belt *CB_3* shows a more evident behaviour of down-tilt migration due to a larger transverse gradient. In contrast, belt *CB_4* underwent shorter evolution (~600 yrs.) and hence developed a smaller width.

Table 1. Parameter settings for the exemplified half-graben model.

Parameter	Distribution	Value
Slip Period	Weibull	μ = 800 yrs. with a range of 100-2000 yrs.
Subsidence Rate	Normal	μ = 0.003 m yr^{-1} with a range of 0.001-0.005 m yr^{-1}
Basin Width Growth Rate	Normal	μ = 0.03 m yr^{-1} with a range of 0.01-0.05 m yr^{-1}
River-channel Width	Constant	60 m
River-channel Depth	Constant	3 m
Minimum Channel-Belt Width	Constant	2000 m
Channel-Belt Lateral Extension Rate	Constant	1 m yr^{-1}
River Avulsion Period	Constant	100 yrs.
Slope Threshold of Channel Lateral Migration	Constant	0.015 °
Slope Threshold of Channel Preferable Relocation	Constant	0.015 °
Buffer Zone Width along Fault	Constant	200 m

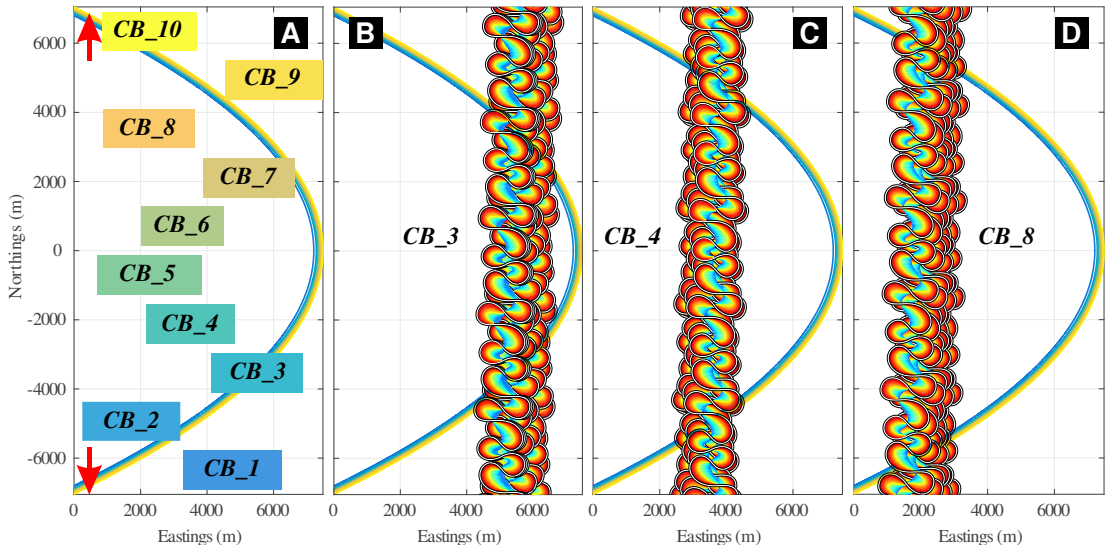

Fig. 9. (A) Locations of modelled meander belts in plan-view, where *CB_10* is the most recent meander belt. The labelled boxes (*CB_1* to *CB_10*) depict the position across the basins where the channel belt developed. For example, *CB_2* was located closest to the basin-bounding fault (i.e. the left-hand edge of the model space, whereas *CB_9* was located furthest from the fault. Each of the ten belts modelled was present through the entire length of the basin. A relatively longer inter-slip period enables development of wider meander belts. Larger basin tilt encourages enhanced rates of lateral migration of the rivers towards the fault. (B-D) Examples of meander belts developed between episodic seismic events. Avulsion is assumed to occur episodically following each seismic event, and the relocation of a river is controlled by the slope of the basin after each slip event.

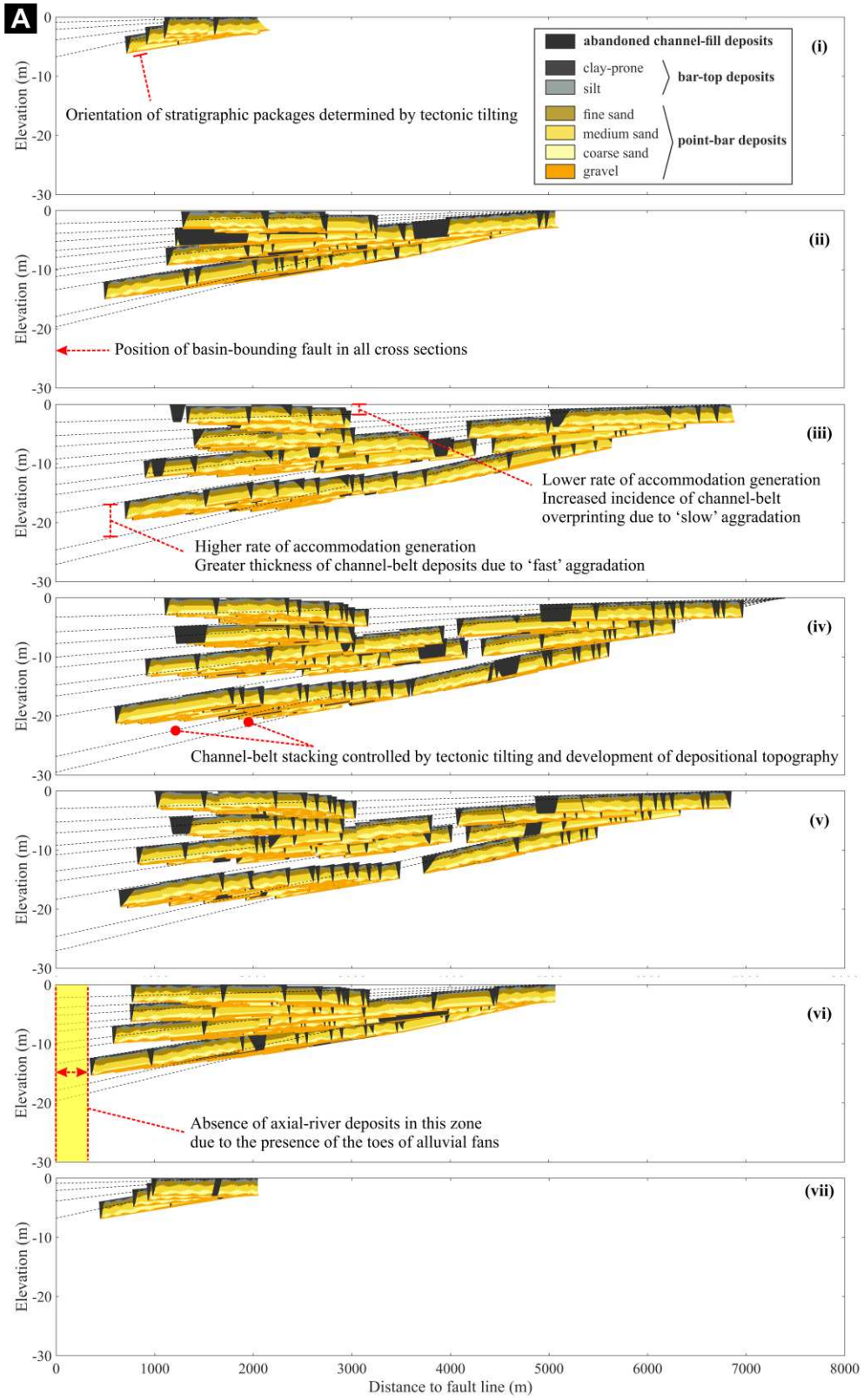

Fig. 10. Two examples of modelled stratigraphic cross sections (perpendicular to the fault line) in 2D after 10 episodes of basin-fill aggradation and channel avulsions induced by tectonic tilting of the half-graben basin. Results of (A) and (B) are from model simulation number 2 and 6 of 10, respectively. See Fig. 8 for location of cross sections. The black dotted lines denote the floodplain surface at the time a tectonic tilting and associated triggered avulsion event occurs. Model results show how the connectivity of point-bar elements changes through the basin and with varying proximity to the bounding fault by different subsidence rates induced by tectonic tilting. [Continued on next page]

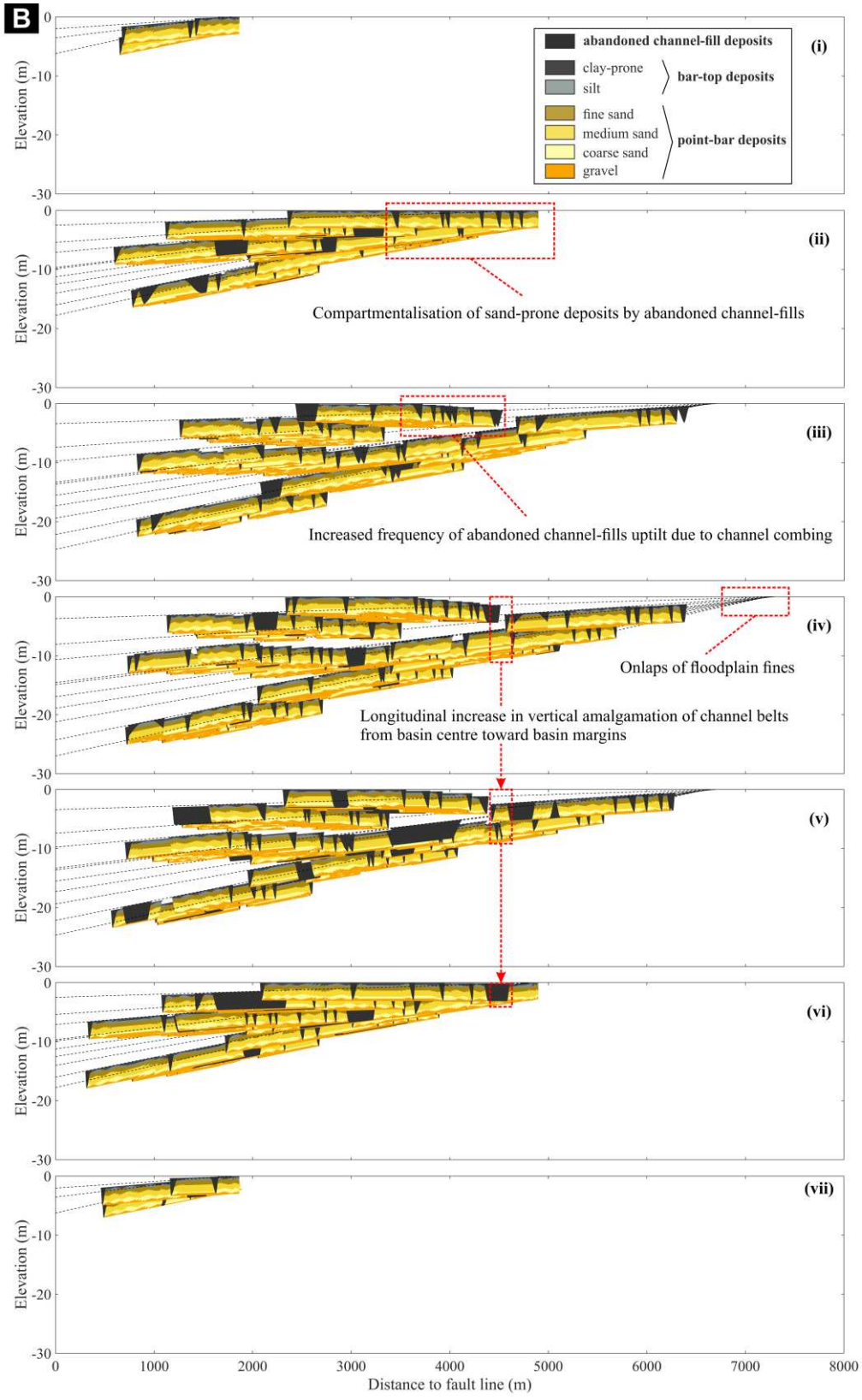

Fig. 10. [Continued from previous page]

Commonly, point-bar deposits within fluvial channel belts mainly comprise sand and gravel, whereas floodplain deposits are dominantly silt and clay (Cant, 1982; Einsele, 2013; Mackey and Bridge, 1992). To take account of a variety of intra-bar facies heterogeneity within point-

bar deposits, six lithofacies arranged in a generally fining-upward trend are herein used to populate the internal facies arrangement of each point-bar element within the model (Fig. 1C-F), including, from bottom to top, gravel (10% in proportion to bar thickness), coarse sand (20%), medium sand (40%), fine sand (10%), silt (10%), and clay (10%). The lithofacies proportions, furthermore, vary stochastically within ±5% of bar thickness to mimic the inherent natural variability observed in nature (Yan *et al.*, 2019). Channel-fill deposits have been modelled as mud-prone units. Representative stratigraphic cross sections perpendicular to the fault strike are presented in Fig. 10 (see also their locations in the 3D frame diagram in Fig. 8B). The maximum subsidence increases from cross section *i* to *iv* and then decreases from cross section *iv* to *vii*. Accordingly, for each cross section, the vertical separation in channel-body tops reflects subsidence variations towards and along the fault. As noted in Fig. 10A*i*, the architecture and orientation of stratigraphic packages is determined by the direction of tectonic tilting. A large transverse gradient encourages faster migration of river channels towards the fault and develop a wider channel belt. Meanwhile, the distance between the channel belts and the fault is constrained by the toes of alluvial fans formed along the fault-strike (Fig. 10A*v*). Accommodation generation controls the rates of channel-belt aggradation. Generation of higher accommodation by a more important seismic event results in more evident channel-belt aggradation (Fig. 10A*iii*). The interplay of tectonic tilting and development of depositional topography determines the resulting channel-belt stacking patterns. Lateral channel migration and combing increases the frequency of abandoned channel-fills uptilt and the compartmentalisation of sand-prone deposits (Fig. 10B*ii*, *iii*). On a basin scale, as accommodation decreases from the basin centre towards margins, amalgamation of channel-belts increases progressively (Fig. 10B*iii*-*v*).

DISTRIBUTION AND CONNECTIVITY OF SAND AND GRAVEL

To examine how the channel-belt stacking patterns vary spatially in a half-graben basin, ten stochastic simulations of basin evolution and fluvial infill were run to take into account intrinsic variability for a given set of boundary conditions. The outputted cross-sections have been rendered as raster images with a horizontal resolution of 8 m and a vertical resolution of 0.05 m, resulting in 8000 × 600 cells in total for each cross section. The six lithofacies types that make up the internal anatomy of the modelled point-bars elements are, furthermore, assigned to two groups: (i) sands and gravels (gravel, and coarse, medium and fine sand) and (ii) muds (silt and clay). This has been done to facilitate analysis of the spatial distribution and connectivity of the relatively porous sand and gravel deposits. The number and size distribution of connected components of sand or gravel (i.e., groups of cells containing sand or gravel and that are connected to each other) was determined for each cross-section of each simulation, using the computer program *GEO_OBJ* (Deutsch, 1998). The occurrence probability of sand-prone lithofacies for each cross section, presented in Fig. 11A, was estimated as an E-map (Remy *et al.*, 2009) based on the frequency of sand-prone lithofacies of each cell at the same coordinates from all ten simulations (Deutsch and Journel, 1998). Sand-prone deposits are less variably distributed, and therefore their presence more predictable, along the cross sections at +/-4000 m from the central section. This is more evident in Figure 11B, which exclusively shows areas where the probability of sand occurrence is greater than 0.5. It also shows that for cross sections closer to the depocentre, the vertical separation of

sand-prone channel-belt deposits is largest, in relation to enhanced preservation of mud-prone bar-top and/or overbank deposits. On the contrary, for a cross section further away from the depocentre, at |*y*| of 4000 m for example, sand-prone channel-belt deposits are well-connected, as available accommodation is more limited and bar tops are more likely to have experienced truncation. These findings are also expressed in the distributions of the number and size of connected sandy and gravelly bodies, presented in Fig. 12. The average number of sand-prone geobodies decreases away from the centre of the basin. The average and median area of the largest sand-prone geobody in each set of cross sections, however, increases first from the central sections to the sections at |*y*| of 2000 m, but then decreases considerably from |*y*| of 4000 m to 6000 m.

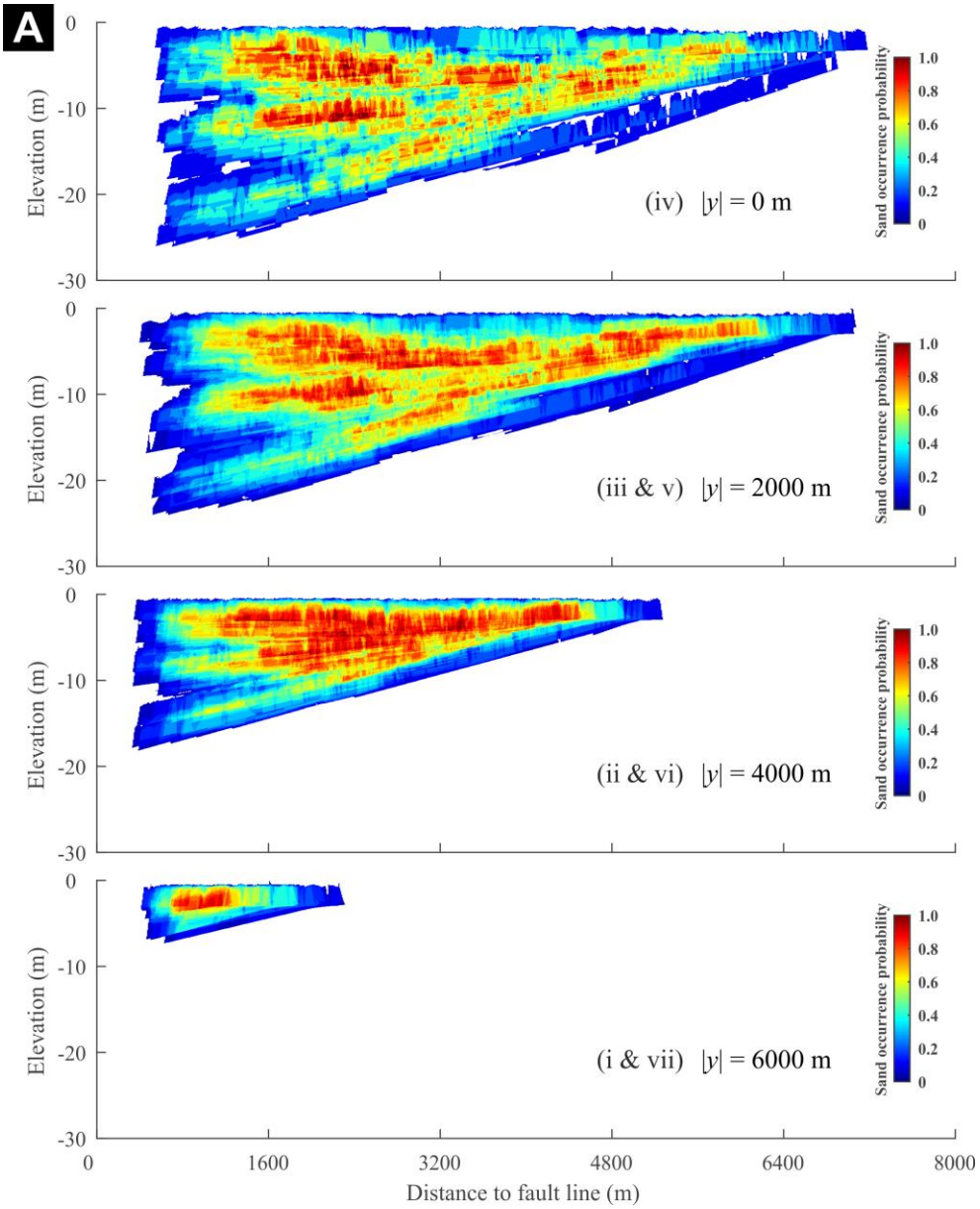

Fig. 11. Cross-sectional maps of the probability of sand or gravel occurrence greater than zero (A) and 0.5 (B) using cross sections from all ten simulations. The resolution is 8 m in the horizontal direction and 0.5 in the vertical direction. See Fig. 8 for location of cross sections. [Continued on next page]

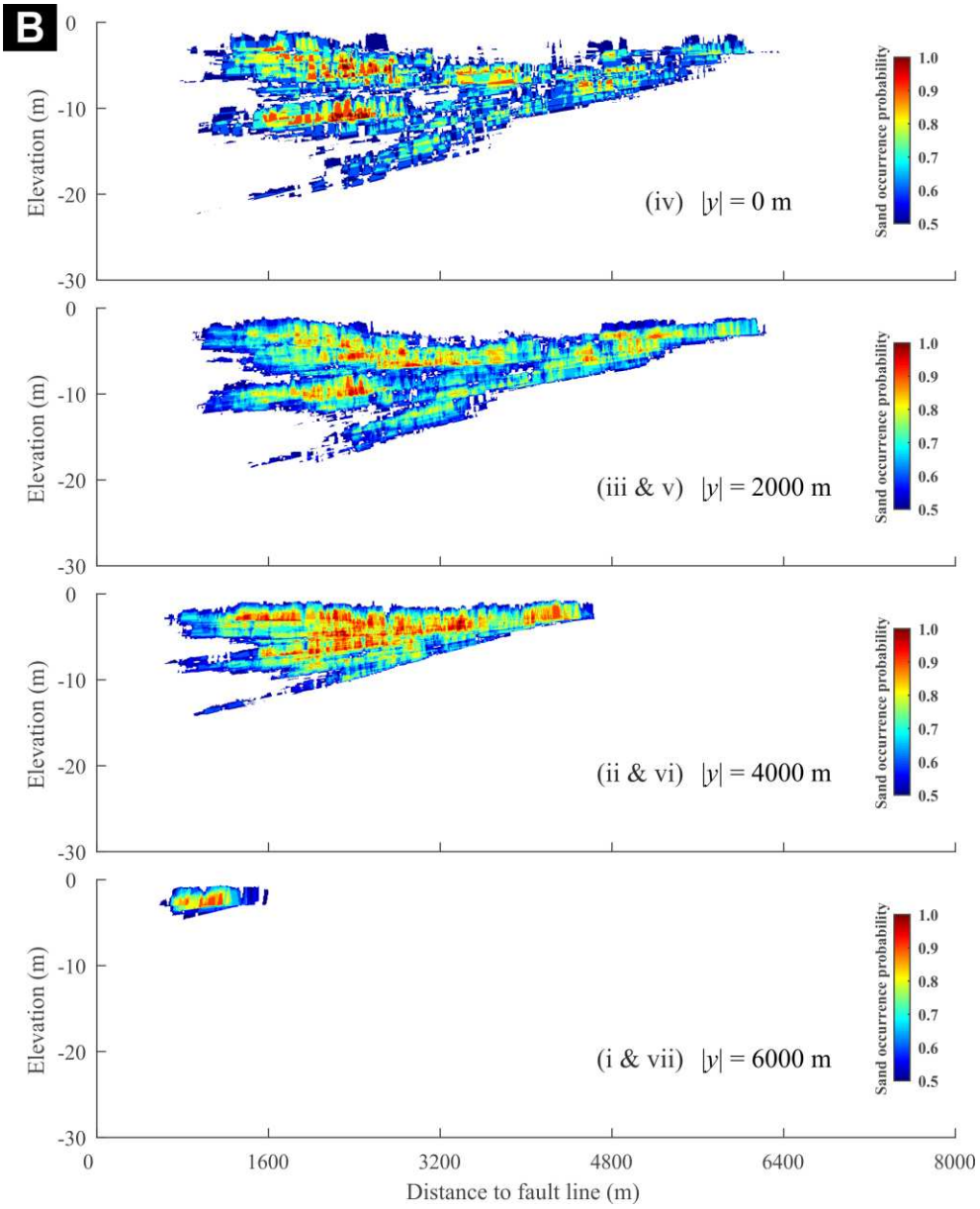

Fig. 11. [Continued from previous page]

DISCUSSION

Scenarios of sedimentary architectures arising from the accumulation of the deposits of meandering river flowing through an evolving half-graben have been modelled numerically using *PB-SAND*. The style of fault evolution, the structural asymmetry of a half-graben, and the magnitude and frequency of hangingwall subsidence exert a great impact on the three-dimensional external morphology and internal stratal geometry and facies heterogeneity of axial channel-belts developed within the evolving basin. These relationships have been effectively captured by the *PB-SAND* models. The point-bar elements modelled in the presented example display expansional and rotational styles of meander transformation, and incorporate fining-upwards and fining-outwards lithofacies trends; thus, the morphological and depositional characteristics typical of fluvial meandering river systems is reproduced. A great

morphological variability exists in the geometrical characteristics of meandering river systems (Blum *et al.*, 2013; Colombera *et al.*, 2017; Milliken *et al.*, 2018); with particular reference to extensional settings, the modelled channel-belts resemble in scale those of the Late Quaternary succession of the Rhine-Meuse delta, the Netherlands, in terms of width (40 - 500 m) and depth (4 - 10 m) of channels and width of the meander-belts (40 - 3200 m) (Cohen *et al.*, 2002).

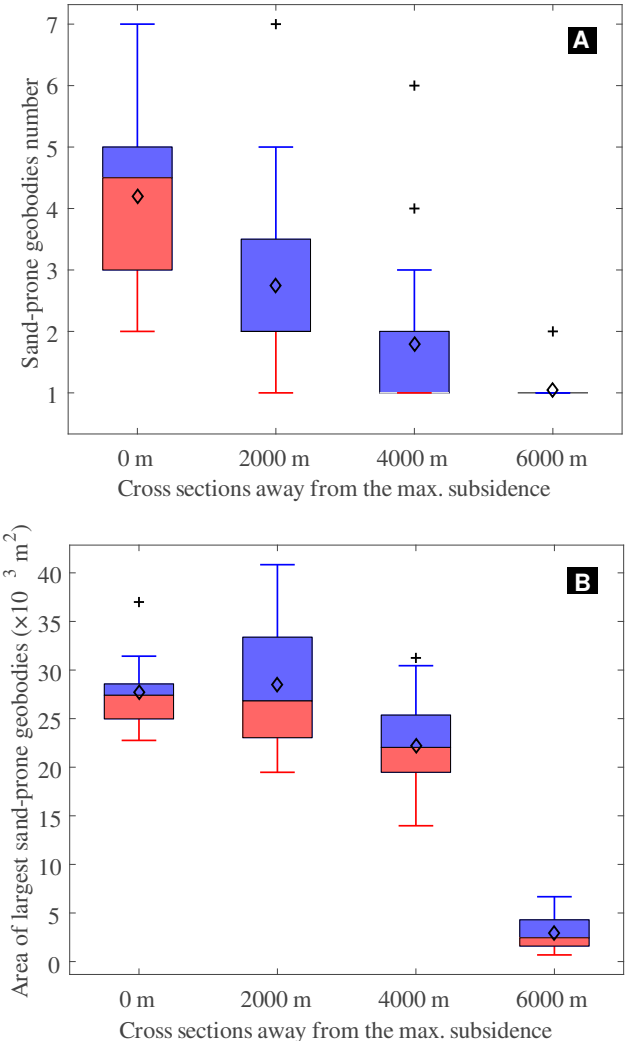

Fig. 12. (A) Box plots of the distribution in the number of sand-prone geobodies in sets of cross sections perpendicular to the fault in a half-graben basin. (B) Box plots of the distribution in the area of largest sand-prone geobodies of cross sections perpendicular to the fault in a half-graben basin. Diamonds represent mean values. The bottom (red) and top (blue) of a box denote the first and third quartiles; the black band inside of the box (between the blue and the red) denotes the median; the whiskers on two sides denote the minimum and maximum values excluding outliers shown as black crosses (outside of 1.5 interquartile range); and the black diamond denotes the mean value.

Spatial variations of hangingwall tilt induced by fault slip and resulting accommodation, the latter expressed as a progressive decrease from the centre of a fault along the fault strike and away from the fault (Chronis *et al.*, 1991), can affect alluvial channel processes and drive lateral migration of channels towards the fault zone; this results in the development of asymmetrical channel-belts in planform, a phenomenon widely found in tectonically controlled meandering river systems (Leeder and Alexander, 1987). The migration rate of channels is directly proportional to the surface gradient perpendicular to the fault, such that steeper gradients result in more asymmetric meander belts, in which the abandoned meander-loops are preferentially preserved uptilt (Leeder and Alexander, 1987); this process is evident in the modelled cross sections in Fig 10. Furthermore, floodplain gradient induced by tectonic tilting also encourages rivers to avulse towards the areas of maximum subsidence adjacent to the fault, leading to clustering of channel belts towards the depocentre, only in part counteracted by compensational

stacking due to depositional topography (Fig. 10). A buffer zone where channel belts cannot develop is employed to mimic the effect of alluvial fans emanating from the footwall (*cf.* Alexander and Leeder, 1987). This buffer zone is kept constant in the model, and the variation induced by complicated interaction between axial river systems and footwall-derived fan systems (Leeder *et al.*, 1996; Leeder and Mack, 2001) is ignored. The river avulsion in the model follows in the aftermath of each tectonic tilting event. This is consistent with the general periodicity of avulsion at the order of $10^2 – 10^3$ years (Aslan *et al.*, 2005; Bridge and Leeder, 1979; Cohen *et al.*, 2002; Peakall, 1998; Schwartz and Coppersmith, 1984), although, more rarely, river avulsions could have a periodicity at the order of 10^4 years (Leeder *et al.*, 1996; Machette *et al.*, 1991). The architecture and facies distribution of the basin fill, by contrast, depend upon a complex interaction between the three-dimensional evolution of the basin, which arises from styles of fault propagation, with processes of river migration and avulsion. As a consequence, a wide range of stratal and facies stacking patterns can develop as a basin evolves, and prediction of the spatial variability and stacking patterns of sandy deposits in the subsurface basin fill remains challenging. As subsidence decreases from the fault towards the basin edges, accommodation decreases and channel-belts are therefore more likely to stack and connect vertically; this effect, however, is counteracted by a reduced probability of occurrence of channel belts, as avulsion is more likely to redirect the river course closer to the fault zone (Fig. 11). Meanwhile, the relative proportions of lithofacies and the internal geometry and heterogeneity of the point-bar elements influence both the location of the maximum volume of sand and gravel ('sweet spot') across the basin (Fig. 10), and the connectivity of these sediments. For example, a higher proportion of mud-prone point-bar deposits requires more significant bar-top erosion in order to attain vertical connections of sand-prone deposits, resulting in a 'sweet spot' located towards the basin edges. Different modes of point-bar sedimentation also control spatial variations of coarse and fine members, for instance because of the development of mud-prone counter-point bar deposits (Ghinassi *et al.*, 2016; Smith *et al.*, 2009). The frequency and spatial continuity of intra-bar mud drapes further increase the complexity in the connectivity of sand-prone geobodies (Colombera *et al.*, 2018; Yan *et al.*, 2019). The number of sand-prone geobodies recognised in sets of cross sections tends to decrease progressively longitudinally along the basin, due to vertical channel-belt amalgamation, as the subsidence decreases progressively from the fault depocentre towards the fault tips (Fig. 12). Instead, the average area of the largest geobody in each cross section increases first away from the depocentre, in response to channel-belt amalgamation, and then decreases markedly, due to the significant decrease of generated accommodation (Fig. 12). A greater overall subsidence rate or a smaller thickness of channel belts will push the location of amalgamated sandy deposits towards the fault tips along a cross section towards the basin edge (Fig. 11). In summary, autogenic river dynamics and allogenic accommodation generation interact in a complex manner, making it difficult to predict the channel-belt stacking patterns in evolving rift basins. *PB-SAND* serves as a tool to examine quantitatively the impacts caused by different geological controls, and can be used to assist in the prediction of the distribution of volumes and of variations in static connectivity in hydrocarbon reservoirs, based on constraints given by seismic and outcrop data.

Limitations of the modelling approach

The growth of the basin appears limited over the modelled period (~10^4 years), in part because only a brief interval of what would have been the entire basin history has been modelled. The resulting basin-fill geometry would vary substantially if modelled at the scale of medium- to longer-term geological time. In particular, as a fault evolves, it may experience multiple stages characteristic of different evolving styles (Fig. 3). Larger faults tend to be confined laterally as displacement continues to accumulate (Gross *et al.*, 1997; Walsh *et al.*, 2002). Moreover, within the model, the position of maximum subsidence on the fault is kept constant through time, which is reasonable considering the short interval being modelled. However, it needs to be considered that the point of maximum subsidence may migrate given a longer period of time (Machette *et al.*, 1991). In the absence of quantitative data regarding the development history of individual faults, the scaling relationship between the accumulated displacement and the fault length by Schlische *et al.* (1996) has been used as a simple assumption for modelling purposes. More realistic simulations could nonetheless be achieved if such temporal data are available as inputs. The displacement rate, meanwhile, varies greatly in different half-graben basins (Table 2), and tends to be underestimated or overestimated due to intrinsic episodic behaviour of seismic activity, and because of phases of active earthquake clustering alternating with quiescent intervals, resulting in significant variability on a wide range of temporal scales (Gawthorpe and Leeder, 2000; Kim and Sanderson, 2005; Machette *et al.*, 1991). Figure 13 shows the distribution of the maximum displacement rate and the maximum subsidence of seismic events from all simulations (100 slips) with a mean of 3.09 mm yr^{-1} and 2.59 m, respectively; these values are comparable to observations from areas with medium seismic activity, for instance, the central graben of the Gulf of Patras in Greece (Chronis *et al.*, 1991). For simplicity, the model presented here has been run based on a set of rules whereby the rate of stream-bed and floodplain aggradation keeps pace with the subsidence rate, such that the accommodation created by each fault-slip event is fully occupied by sediment before the subsequent slip event. In reality, accommodation generation could be more rapid than the rate at which a river system attains equilibrium, at least over certain timescales, and alternative model runs could be tailored to account for this. Additionally, the model is also based on the assumption that the hangingwall substrate is as erodible as the basin fill: this may not be realistic in many cases.

Table. 2. Examples of subsidence rates of half-graben rift basins.

Half-graben system	Displacement rate	Reference
Gulf of Patras, Greece	1-5 mm yr^{-1}	Chronis *et al.* (1991)
Argolikos Gulf, Greece	0.5-1.0 mm yr^{-1}	Van Andel *et al.* (1993)
Wasatch fault zone, Utah, USA	<2 mm yr^{-1}	Schwartz and Coppersmith (1984)
Rio Grande rift, New Mexico, USA	0.03 mm yr^{-1}	Leeder *et al.* (1996)
Genoa Fault, Carson Valley, Nevada, USA	0.48 - 0.8 mm yr^{-1}	Peakall (1998)
Roer Valley, Rhine-Meuse delta, Netherlands	0.09 to 0.15 mm yr^{-1}	Cohen *et al.* (2002)

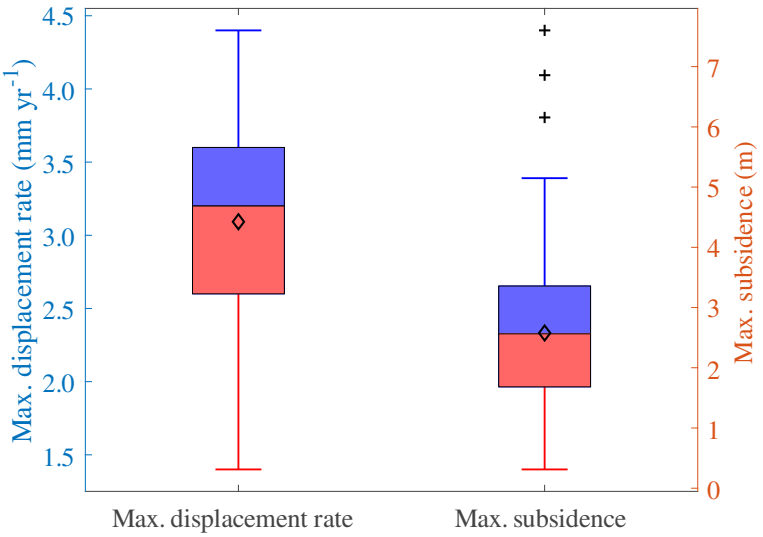

Fig. 13. The maximum displacement rate and subsidence from ten simulations, each of which includes ten episodic slip events, resulting in 100 slip events in total. Diamonds represent mean values. The bottom (red) and top (blue) of a box denote the first and third quartiles; the black band inside of the box (between the blue and the red) denotes the median; the whiskers on two sides denote the minimum and maximum values excluding outliers shown as black crosses (outside of 1.5 interquartile range); and the black diamond denotes the mean value.

In the results presented herein, modelled architectures of basin fill arise as a response to channel-belt avulsion that occurred with each slip event. In natural systems, minor slip events might not necessarily result in reach avulsion. Rather, they might merely result in a shift in the trend of the channel path as the local surface gradient changes. Moreover, in the scenario modelled here avulsion events take place upstream of the basin. Alternative scenarios could be modelled where avulsion events occur within the confines of the evolving basin, thereby allowing greater flexibility in simulating the timing and location of avulsion events (Fig. 7).
For purposes of computational efficiency, amalgamated channel belts are modelled as the product of the vertical overlap of simple channel belts with offset tops; this results in simplified internal architectures of meander belts, though it has no appreciable effect on the overall connectivity of the channel fill sand bodies at the basin scale (Figs 10 and 11). Lateral offset of the same channel belts is used to model preferential river migration towards the basin-bounding fault, resulting in combing abandoned loops being dominantly preserved up the hangingwall dip slope. Yet, in the modelled examples, oxbow-shaped abandoned channel fills that are compatible – in terms of position, shape, and stratigraphic relationship – with 'recent' cut off having occurred in the pre-avulsion evolution of the channel belt are notably lacking. This is because the same channel-belt pattern has been replicated throughout the model for simplicity in the modelled scenarios presented. For more complicated basin-fill scenarios, the PB-SAND model is capable of accounting for oxbow-shaped abandoned channel fills; the stratigraphic complexity of such features can be incorporated by capturing planform patterns from a wider library of known stratigraphic patterns and by incorporating cut-off channel fills.

CONCLUSIONS

A forward stratigraphic model (*PB-SAND*) has been used to explore the spatio-temporal evolution and stacking patterns of fluvial channel-belt deposits that form the fill of an evolving half-graben basin. The modelled half-graben represents an idealised case, based on metrics of

basin characteristics compatible with natural examples. The modelled scenarios are comparable to geological analogues in terms of the trajectories of fault development triggered by seismic-induced slip events, the style of fault propagation, the episodic pivot-like motion of the hangingwall, the avulsion frequency of channel belts, the rate and style of migration of river channels, and the planform morphology, internal heterogeneity and stacking patterns of channel-belt deposits. The *PB-SAND* model can facilitate quantitative examination of variations in facies heterogeneity and sand connectivity in fluvial successions in rift basins, by assessing the relative significance of input parameters that mimic allogenic and autogenic processes, thus allowing exploration of the influence of geological boundary conditions on fluvial sedimentary architecture at different scales. The *PB-SAND* model can be used as a predictive tool in hydrocarbon exploration, in specific cases informed by outcrop, seismic, and/or borehole data. Notably, model results can be used to predict sandbody distribution and connectivity. This modelling approach describes a novel method to account for combined sedimentological and tectonic controls on basin-fill sedimentary architecture across a range of spatial and temporal scales. The novel approach and methodology developed as part of this research finds application in hydrocarbon reservoir exploration, prediction and development. Furthermore, this approach can be used to characterise groundwater aquifers, and also finds use in assessment of basin-fill successions being considered as long-term repositories in underground carbon sequestration projects or for exploitation of geothermal resources.

ACKNOWLEDGEMENTS

The authors thank Nexen Energy ULC, Canada, for provision of financial support for development of *PB-SAND*, and FRG-ERG sponsors (AkerBP, Areva, BHPBilliton, Cairn India [Vedanta], Chevron, ConocoPhillips, Murphy Oil, Nexen Energy, Saudi Aramco, Shell, Tullow Oil, Woodside, and YPF) and our partner Petrotechnical Data Systems for financial support of the research group. Elisabetta Bosi is thanked for research assistance. Adrian Hartley and two anonymous reviewers are thanked for their constructive comments which have greatly improved this manuscript.

REFERENCES

ALEXANDER, J. & LEEDER, M.R. (1987) Active Tectonic Control on Alluvial Architecture. In: *Recent Developments in Fluvial Sedimentology* (Ed. by F. G. Ethridge, R. M. Flores & M. D. Harvey), 243-252. SEPM Special Publication 39.

ALEXANDER, J., BRIDGE, J.S., LEEDER, M.R., COLLIER, R.E.L. & GAWTHORPE, R.L. (1994) Holocene Meander-Belt Evolution in an Active Extensional Basin, Southwestern Montana. *Journal of Sedimentary Research*, **64**.

ANDERSON, R.E., ZOBACK, M.L. & THOMPSON, G.A. (1983) Implications of Selected Subsurface Data on the Structural Form and Evolution of Some Basins in the Northern Basin and Range Province, Nevada and Utah. *Geological Society of America Bulletin*, **94,** 1055-1072.

ARMSTRONG, C., MOHRIG, D., HESS, T., GEORGE, T. & STRAUB, K.M. (2014) Influence of Growth Faults on Coastal Fluvial Systems: Examples from the Late Miocene to Recent Mississippi River Delta. *Sedimentary Geology*, **301,** 120-132.

ASLAN, A., AUTIN, W.J. & BLUM, M.D. (2005) Causes of River Avulsion: Insights from the Late Holocene Avulsion History of the Mississippi River, USA. *Journal of Sedimentary Research*, **75,** 650-664.

BACHU, S. (2000) Sequestration of Co2 in Geological Media: Criteria and Approach for Site Selection in Response to Climate Change. *Energy Conversion and Management*, **41,** 953-970.

BANHAM, S.G. & MOUNTNEY, N.P. (2013) Controls on Fluvial Sedimentary Architecture and Sediment-Fill State in Salt-Walled Mini-Basins: Triassic Moenkopi Formation, Salt Anticline Region, Se Utah, USA. *Basin Research*, **25,** 709-737.

BATH, A., RICHARDS, H., METCALFE, R., MCCARTNEY, R., DEGNAN, P. & LITTLEBOY, A. (2006) Geochemical Indicators of Deep Groundwater Movements at Sellafield, Uk. *Journal of Geochemical Exploration*, **90,** 24-44.

BISWAS, S.K. (2003) Regional Tectonic Framework of the Pranhita–Godavari Basin, India. *Journal of Asian Earth Sciences*, **21,** 543-551.

BLUM, M., MARTIN, J., MILLIKEN, K. & GARVIN, M. (2013) Paleovalley Systems: Insights from Quaternary Analogs and Experiments. *Earth-Science Reviews*, **116,** 128-169.

BONINI, L., BASILI, R., TOSCANI, G., BURRATO, P., SENO, S. & VALENSISE, G. (2016) The Effects of Pre-Existing Discontinuities on the Surface Expression of Normal Faults: Insights from Wet-Clay Analog Modeling. *Tectonophysics*, **684,** 157-175.

BRIDGE, J.S. & LEEDER, M.R. (1979) A Simulation Model of Alluvial Stratigraphy. *Sedimentology*, **26,** 617-644.

BÜRGMANN, R., POLLARD, D.D. & MARTEL, S.J. (1994) Slip Distributions on Faults: Effects of Stress Gradients, Inelastic Deformation, Heterogeneous Host-Rock Stiffness, and Fault Interaction. *Journal of Structural Geology*, **16,** 1675-1690.

CANT, D.J. (1982) Fluvial Facies Models and Their Application. In: *Sandstone Depositional Environments* (ed. by Horn, M.K.) American Association of Petroleum Geologists Memoir 31, 115-137.

CARTER, K.E. & WINTER, C.L. (1995) Fractal Nature and Scaling of Normal Faults in the Española Basin, Rio Grande Rift, New Mexico: Implications for Fault Growth and Brittle Strain. *Journal of Structural Geology*, **17,** 863-873.

CARTWRIGHT, J.A., TRUDGILL, B.D. & MANSFIELD, C.S. (1995) Fault Growth by Segment Linkage: An Explanation for Scatter in Maximum Displacement and Trace Length Data from the Canyonlands Grabens of Se Utah. *Journal of Structural Geology*, **17,** 1319-1326.

CHRONIS, G., PIPER, D.J.W. & ANAGNOSTOU, C. (1991) Late Quaternary Evolution of the Gulf of Patras, Greece: Tectonism, Deltaic Sedimentation and Sea-Level Change. *Marine Geology*, **97,** 191-209.

CLARK, R.M. & COX, S.J.D. (1996) A Modern Regression Approach to Determining Fault Displacement-Length Scaling Relationships. *Journal of Structural Geology*, **18,** 147-152.

COHEN, K.M., STOUTHAMER, E. & BERENDSEN, H.J.A. (2002) Fluvial Deposits as a Record for Late Quaternary Neotectonic Activity in the Rhine-Meuse Delta, the Netherlands. *Netherlands Journal of Geosciences - Geologie en Mijnbouw*, **81,** 389-405.

COLEMAN, J.M. (1969) Brahmaputra River: Channel Processes and Sedimentation. *Sedimentary Geology*, **3,** 129-239.

COLOMBERA, L., MOUNTNEY, N.P., RUSSELL, C.E., SHIERS, M.N. & MCCAFFREY, W.D. (2017) Geometry and Compartmentalization of Fluvial Meander-Belt Reservoirs at the Bar-Form Scale: Quantitative Insight from Outcrop, Modern and Subsurface Analogues. *Marine and Petroleum Geology*, **82,** 35-55.

COLOMBERA, L., YAN, N., MCCORMICK-COX, T. & MOUNTNEY, N.P. (2018) Seismic-Driven Geocellular Modeling of Fluvial Meander-Belt Reservoirs Using a Rule-Based Method. *Marine and Petroleum Geology*, **93**, 553-569.

CORBETT, P.W., HAMDI, H. & GURAV, H. (2012) Layered Fluvial Reservoirs with Internal Fluid Cross Flow: A Well-Connected Family of Well Test Pressure Transient Responses. *Petroleum Geoscience*, **18,** 219-229.

COWIE, P.A. & SCHOLZ, C.H. (1992) Physical Explanation for the Displacement-Length Relationship of Faults Using a Post-Yield Fracture Mechanics Model. *Journal of Structural Geology*, **14,** 1133-1148.

COWIE, P.A., GUPTA, S. & DAWERS, N.H. (2000) Implications of Fault Array Evolution for Synrift Depocentre Development: Insights from a Numerical Fault Growth Model. *Basin Research*, **12,** 241-261.

DAWERS, N.H., ANDERS, M.H. & SCHOLZ, C.H. (1993) Growth of Normal Faults: Displacement-Length Scaling. *Geology*, **21,** 1107-1110.

DAWERS, N.H. & ANDERS, M.H. (1995) Displacement-Length Scaling and Fault Linkage. *Journal of Structural Geology*, **17,** 607-614.

DEUTSCH, C.V. (1998) Fortran Programs for Calculating Connectivity of Three-Dimensional Numerical Models and for Ranking Multiple Realizations. *Computers & Geosciences*, **24,** 69-76.

DEUTSCH, C.V. & JOURNEL, A.G. (1998) Geostatistical Software Library and User's Guide. *Oxford University Press, New York*.

DIXON, S.J., SAMBROOK SMITH, G.H., BEST, J.L., NICHOLAS, A.P., BULL, J.M., VARDY, M.E., SARKER, M.H. & GOODBRED, S. (2018) The Planform Mobility of River Channel Confluences: Insights from Analysis of Remotely Sensed Imagery. *Earth-Science Reviews*, **176,** 1-18.

EINSELE, G. (2013) *Sedimentary Basins: Evolution, Facies, and Sediment Budget*. Springer Science & Business Media.

FILBRANDT, J., RICHARD, P. & FRANSSEN, R. (1994). *Growth and Coalescence of Faults: Numerical Simulations and Sand-Box Experiments*. TSG Special Meeting on Fault Populations, Edinburgh, UK, Extended Abstract, Tectonic Studies Group.

FISK, H.N. (1944) Geological Investigation of the Alluvial Valley of the Lower Mississippi River. *U.S. Department of the Army, Mississippi River Commission***,** 78.

FRASER, G.S., THOMPSON, T.A., OLYPHANT, G.A., FURER, L. & BENNETT, S.W. (1997) Geomorphic Response to Tectonically-Induced Ground Deformation in the Wabash Valley. *Seismological Research Letters*, **68,** 662-674.

FUSTIC, M., HUBBARD, S.M., SPENCER, R., SMITH, D.G., LECKIE, D.A., BENNETT, B. & LARTER, S. (2012) Recognition of Down-Valley Translation in Tidally Influenced Meandering Fluvial Deposits, Athabasca Oil Sands (Cretaceous), Alberta, Canada. *Marine and Petroleum Geology*, **29,** 219-232.

GAWTHORPE, R.L., FRASER, A.J. & COLLIER, R.E.L. (1994) Sequence Stratigraphy in Active Extensional Basins: Implications for the Interpretation of Ancient Basin-Fills. *Marine and Petroleum Geology*, **11,** 642-658.

GAWTHORPE, R.L. & LEEDER, M.R. (2000) Tectono-Sedimentary Evolution of Active Extensional Basins. Basin Research, 195–218.

GHAZI, S. & MOUNTNEY, N.P. (2009) Facies and Architectural Element Analysis of a Meandering Fluvial Succession: The Permian Warchha Sandstone, Salt Range, Pakistan. Sedimentary Geology, **221**, 99-126.

GHINASSI, M., NEMEC, W., ALDINUCCI, M., NEHYBA, S., ÖZAKSOY, V. & FIDOLINI, F. (2014) Plan-Form Evolution of Ancient Meandering Rivers Reconstructed from Longitudinal Outcrop Sections. *Sedimentology*, **61,** 952-977.

GHINASSI, M. & IELPI, A. (2015) Stratal Architecture and Morphodynamics of Downstream-Migrating Fluvial Point Bars (Jurassic Scalby Formation, U.K.). *Journal of Sedimentary Research*, **85,** 1123-1137.

GHINASSI, M., IELPI, A., ALDINUCCI, M. & FUSTIC, M. (2016) Downstream-Migrating Fluvial Point Bars in the Rock Record. *Sedimentary Geology*, **334,** 66-96.

GILLESPIE, P.A., WALSH, J.J. & WATTERSON, J. (1992) Limitations of Dimension and Displacement Data from Single Faults and the Consequences for Data Analysis and Interpretation. *Journal of Structural Geology*, **14,** 1157-1172.

GROSS, M.R., GUTIE, G., BAI, T., WACKER, M.A., COLLINSWORTH, K.B. & BEHL, R.J. (1997) Influence of Mechanical Stratigraphy and Kinematics on Fault Scaling Relations. *Journal of Structural Geology*, **19,** 171-183.

GUDMUNDSSON, A. (2005) Effects of Mechanical Layering on the Development of Normal Faults and Dykes in Iceland. *Geodinamica Acta*, **18,** 11-30.

GUDMUNDSSON, A., DE GUIDI, G. & SCUDERO, S. (2013) Length–Displacement Scaling and Fault Growth. *Tectonophysics*, **608,** 1298-1309.

HAGIWARA, Y. (1974) Probability of Earthquake Occurrence as Obtained from a Weibull Distribution Analysis of Crustal Strain. *Tectonophysics*, **23,** 313-318.

HAJEK, E.A., HELLER, P.L. & SHEETS, B.A. (2010) Significance of Channel-Belt Clustering in Alluvial Basins. *Geology*, **38,** 535-538.

HAMDI, H., RUELLAND, P., BERGEY, P. & CORBETT, P.W. (2014) Using Geological Well Testing for Improving the Selection of Appropriate Reservoir Models. *Petroleum Geoscience***,** 2012-2074.

IELPI, A. & GHINASSI, M. (2014) Planform Architecture, Stratigraphic Signature and Morphodynamics of an Exhumed Jurassic Meander Plain (Scalby Formation, Yorkshire, Uk). *Sedimentology*, **61,** 1923-1960.

JACKSON, J. (1987) Active Normal Faulting and Crustal Extension. *Geological Society, London, Special Publications*, **28,** 3-17.

JOLLEY, S.J., FISHER, Q.J. & AINSWORTH, R.B. (2010) Reservoir Compartmentalization: An Introduction. *Geological Society, London, Special Publications*, **347,** 1-8.

KIM, Y.-S. & SANDERSON, D.J. (2005) The Relationship between Displacement and Length of Faults. *Earth-Science Reviews*, **68,** 317-334.

LARUE, D.K. & HOVADIK, J. (2006) Connectivity of Channelized Reservoirs: A Modelling Approach. *Petroleum Geoscience*, **12,** 291-308.

LEEDER, M.R. & ALEXANDER, J.A.N. (1987) The Origin and Tectonic Significance of Asymmetrical Meander-Belts. *Sedimentology*, **34,** 217-226.

LEEDER, M.R. & GAWTHORPE, R.L. (1987) Sedimentary Models for Extensional Tilt-Block/Half-Graben Basins. In: *Continental Extensional Tectonics* (Ed. by M. P. Coward, J. F. Dewey & P. L. Hancock). Geological Society Special Publication 28, 139-152

LEEDER, M.R. & MACK, G.H. (2001) Lateral Erosion (Toe-Cutting) of Alluvial Fans by Axial Rivers: Implications for Basin Analysis and Architecture. *Journal of the Geological Society*, **158**, 885-893.

LEEDER, M.R., MACK, G.H., PEAKALL, J. & SALYARDS, S.L. (1996) First Quantitative Test of Alluvial Stratigraphic Models: Southern Rio Grande Rift, New Mexico. *Geology*, **24,** 87-90.

LEEDER, M., MACK, G. & SALYARDS, S. (1996) Axial–Transverse Fluvial Interactions in Half-Graben: Plio-Pleistocene Palomas Basin, Southern Rio Grande Rift, New Mexico, USA. Basin Research, **8**, 225-241.

LEEDER, M.R. (2011) Tectonic Sedimentology: Sediment Systems Deciphering Global to Local Tectonics. *Sedimentology*, **58,** 2-56.

LOCKWOOD, J.G. (2001) Abrupt and Sudden Climatic Transitions and Fluctuations: A Review. *International Journal of Climatology*, **21,** 1153-1179.

MACHETTE, M.N., PERSONIUS, S.F., NELSON, A.R., SCHWARTZ, D.P. & LUND, W.R. (1991) The Wasatch Fault Zone, Utah—Segmentation and History of Holocene Earthquakes. *Journal of Structural Geology*, **13,** 137-149.

MACK, G.H. & LEEDER, M.R. (1999) Climatic and Tectonic Controls on Alluvial-Fan and Axial-Fluvial Sedimentation in the Plio-Pleistocene Palomas Half Graben, Southern Rio Grande Rift. *Journal of Sedimentary Research*, **69,** 635-652.

MACKEY, S.D. & BRIDGE, J.S. (1992) A Revised Fortran Program to Simulate Alluvial Stratigraphy. *Computers & Geosciences*, **18,** 119-181.

MARRETT, R. & ALLMENDINGER, R.W. (1991) Estimates of Strain Due to Brittle Faulting: Sampling of Fault Populations. *Journal of Structural Geology*, **13,** 735-738.

MCDONALD, R.E. (1976) Tertiary Tectonics and Sedimentary Rocks Along the Transition: Basin and Range Province to Plateau and Thrust Belt Province, Utah.

MEDICI, G., WEST, L. & MOUNTNEY, N. (2016) Characterizing Flow Pathways in a Sandstone Aquifer: Tectonic Vs Sedimentary Heterogeneities. *Journal of Contaminant Hydrology*, **194,** 36-58.

MEDICI, G., WEST, L. & MOUNTNEY, N. (2018a) Characterization of a Fluvial Aquifer at a Range of Depths and Scales: The Triassic St Bees Sandstone Formation, Cumbria, Uk. *Hydrogeology Journal*, **26,** 565-591.

MEDICI, G., WEST, L.J. & MOUNTNEY, N.P. (2018b) Sedimentary Flow Heterogeneities in the Triassic Uk Sherwood Sandstone Group: Insights for Hydrocarbon Exploration. *Geological Journal*.

MILLIKEN, K.T., BLUM, M.D., SNEDDEN, J.W. & GALLOWAY, W.E. (2018) Application of Fluvial Scaling Relationships to Reconstruct Drainage-Basin Evolution and Sediment Routing for the Cretaceous and Paleocene of the Gulf of Mexico. *Geosphere*, **14,** 749-767.

MORETTI, I., SAKELLARIOU, D., LYKOUSIS, V. & MICARELLI, L. (2003) The Gulf of Corinth: An Active Half Graben? *Journal of Geodynamics*, **36,** 323-340.

NICOL, A., WALSH, J., WATTERSON, J. & GILLESPIE, P. (1996) Fault Size Distributions—Are They Really Power-Law? *Journal of Structural Geology*, **18,** 191-197.

PEACOCK, D. & SANDERSON, D. (1996) Effects of Propagation Rate on Displacement Variations Along Faults. *Journal of Structural Geology*, **18,** 311-320.

PEACOCK, D. (2002) Propagation, Interaction and Linkage in Normal Fault Systems. *Earth-Science Reviews*, **58,** 121-142.

PEAKALL, J. (1998) Axial River Evolution in Response to Half-Graben Faulting: Carson River, Nevada, USA. *Journal of Sedimentary Research*, **68**.

PEAKALL, J., LEEDER, M., BEST, J. & ASHWORTH, P. (2000) River Response to Lateral Ground Tilting: A Synthesis and Some Implications for the Modelling of Alluvial Architecture in Extensional Basins. *Basin Research*, **12,** 413-424.

PICKERING, G., BULL, J.M. & SANDERSON, D.J. (1995) Sampling Power-Law Distributions. *Tectonophysics*, **248,** 1-20.

REID, J. & JOHN, B. (1992) The Owens River as a Tiltmeter for Long Valley Caldera, California. *The Journal of Geology*, **100,** 353-363.

REMY, N., BOUCHER, A. & WU, J. (2009) *Applied Geostatistics with Sgems: A User's Guide*. Cambridge University Press, Cambridge.

RING, U., BETZLER, C. & DELVAUX, D. (1992) Normal Vs Strike-Slip Faulting During Rift Development in East-Africa - the Malawi Rift. *Geology*, **20,** 1015-1018.

RUSS, D.P. (1982) Style and Significance of Surface Deformation in the Vicinity of New Madrid, Missouri.

RUSSELL, C.E., MOUNTNEY, N.P., HODGSON, D.M. & COLOMBERA, L. (2019) A Novel Approach for Prediction of Lithological Heterogeneity in Fluvial Point ‐ Bar Deposits from Analysis of Meander Morphology and Scroll-Bar Pattern. In: *Meandering Rivers and Their Depositional Record* (Ed. by M. Ghinassi, N. Mountney, L. Colombera & A. J. Reesink), Special Publication 48 of the International Association of Sedimentologists, 385-418.

SCHLISCHE, R.W. (1991) Half-Graben Basin Filling Models: New Constraints on Continental Extensional Basin Development. *Basin Research*, **3,** 123-141.

SCHLISCHE, R.W. & ANDERS, M.H. (1996) Stratigraphic Effects and Tectonic Implications of the Growth of Normal Faults and Extensional Basins. *Special papers – Geological Society of Society of America*, 183-203.

SCHLISCHE, R.W. & OLSEN, P.E. (1990) Quantitative Filling Model for Continental Extensional Basins with Applications to Early Mesozoic Rifts of Eastern North America. *The Journal of Geology*, **98**, 135-155.

SCHLISCHE, R.W., YOUNG, S.S., ACKERMANN, R.V. & GUPTA, A. (1996) Geometry and Scaling Relations of a Population of Very Small Rift-Related Normal Faults. *Geology*, **24,** 683-686.

SCHOLZ, C.H. & COWIE, P.A. (1990) Determination of Total Strain from Faulting Using Slip Measurements. *Nature*, **346,** 837.

SCHOLZ, C.H., DAWERS, N.H., YU, J.Z., ANDERS, M.H. & COWIE, P.A. (1993) Fault Growth and Fault Scaling Laws: Preliminary Results. *Journal of Geophysical Research: Solid Earth*, **98,** 21951-21961.

SCHWARTZ, D.P. & COPPERSMITH, K.J. (1984) Fault Behavior and Characteristic Earthquakes: Examples from the Wasatch and San Andreas Fault Zones. *Journal of Geophysical Research: Solid Earth*, **89,** 5681-5698.

SEGALL, P. & POLLARD, D. (1980) Mechanics of Discontinuous Faults. *Journal of Geophysical Research: Solid Earth*, **85,** 4337-4350.

SMITH, D.G., HUBBARD, S.M., LECKIE, D.A. & FUSTIC, M. (2009) Counter Point Bar Deposits: Lithofacies and Reservoir Significance in the Meandering Modern Peace River and Ancient Mcmurray Formation, Alberta, Canada. *Sedimentology*, **56,** 1655-1669.

STOUTHAMER, E. & BERENDSEN, H.J. (2001) Avulsion Frequency, Avulsion Duration, and Interavulsion Period of Holocene Channel Belts in the Rhine-Meuse Delta, the Netherlands. *Journal of Sedimentary Research*, **71,** 589-598.

TELLAM, J.H. & BARKER, R.D. (2006) Towards Prediction of Saturated-Zone Pollutant Movement in Groundwaters in Fractured Permeable-Matrix Aquifers: The Case of the Uk Permo-Triassic Sandstones. *Geological Society, London, Special Publications*, **263,** 1-48.

VAN ANDEL, T.H., PERISSORATIS, C. & RONDOYANNI, T. (1993) Quaternary Tectonics of the Argolikos Gulf and Adjacent Basins, Greece. *Journal of the Geological Society*, **150,** 529-539.

VILLEMIN, T., ANGELIER, J. & SUNWOO, C. (1995) Fractal Distribution of Fault Length and Offsets: Implications of Brittle Deformation Evaluation—the Lorraine Coal Basin. In: *Fractals in the Earth Sciences* (Ed. by C. C. Barton & P. R. La Pointe), 205-226. Springer US, Boston, MA.

WALSH, J. & WATTERSON, J. (1987) Distributions of Cumulative Displacement and Seismic Slip on a Single Normal Fault Surface. *Journal of Structural Geology*, **9,** 1039-1046.

WALSH, J., NICOL, A. & CHILDS, C. (2002) An Alternative Model for the Growth of Faults. *Journal of Structural Geology*, **24,** 1669-1675.

WALSH, J.J. & WATTERSON, J. (1988) Analysis of the Relationship between Displacements and Dimensions of Faults. *Journal of Structural Geology*, **10,** 239-247.

WATTERSON, J. (1986) Fault Dimensions, Displacements and Growth. *pure and applied geophysics*, **124,** 365-373.

WITHJACK, M.O., SCHLISCHE, R.W. & OLSEN, P.E. (2002) Rift-Basin Structure and Its Influence on Sedimentary Systems.

YAN, N., MOUNTNEY, N.P., COLOMBERA, L. & DORRELL, R.M. (2017) A 3d Forward Stratigraphic Model of Fluvial Meander-Bend Evolution for Prediction of Point-Bar Lithofacies Architecture. *Computers & Geosciences*, **105,** 65-80.

YAN, N., COLOMBERA, L., MOUNTNEY, N. & DORRELL, R.M. (2019) Fluvial Point-Bar Architecture and Facies Heterogeneity, and Their Influence on Intra-Bar Static Connectivity in Humid Coastal-Plain and Dryland Fan Systems. In: *Meandering Rivers and Their Depositional Record* (Ed. by M. Ghinassi, N. Mountney, L. Colombera & A. J. Reesink), Special Publication 48 of the International Association of Sedimentologists, 475-508.